Addis Ababa University
Addis Ababa Institute of Technology
African Railway Center of Excellence

PHOTOVOLTAIC AND ENERGY STORAGE DESIGN FOR AUXILIARY LOADS OF ELECTRIC LIGHT WEIGHT TRAIN: CASE OF ADDIS ABABA LIGHT RAIL TRANSIT

A Research Thesis Submitted to the School of Graduate Studies of Addis Ababa University in Partial Fulfillment of the Requirements for the Degree of Master of Science in Railway Engineering (Traction and Train Control)

Regis Nibaruta

Advisor: Mengesha Mamo (PhD)

August 2021
Addis Ababa
Ethiopia

Approval

The undersigned have examined the thesis entitled **"Photovoltaic and Energy Storage design for Auxiliary Loads of electric light weight train: case of Addis Ababa Light Rail Transit."** Presented by Regis NIBARUTA of registration number GSR/4769/12, A thesis submitted to African Railway Center of Excellence, Addis Ababa Institute of Technology, School of Graduate Studies in partial fulfilment of the requirement of the award of Degree of Master of Science in Railway Engineering (Traction and Train Control).

Submitted by:

Regis Nibaruta	.....	09/08/2021
Student	Signature	Date

Approved by:

Mengesha Mamo (PhD)	.....	12.08.2021
Advisor	Signature	Date
Getachew Biru Worku (PhD)	.....	09.08.21
Examiner 1	Signature	Date
Mr. Alula Mebratu	.....	10/08/2021
Examiner 2	Signature	Date
Mr. Birhanu Reesom Bistrat	.....	16/08/2021
Chairperson	Signature	Date

Director of Postgraduate Program

Addis Ababa Institute of Technology

Declaration

This thesis is my original work, except where due acknowledgement is made in the text, and to the best of my knowledge has not been previously submitted to Addis Ababa University or any other institutions for the award of a degree.

Signature: ..... Date: 09/08/2021

REGIS NIBARUTA

Abstract

In recent decades, the world has turned its attention to renewable energy supply in an attempt to fight climate change and global warming. While renewable energy provides a cleaner and less expensive energy source, it is critical to assess the possibility of installing of solar PV systems with storage on electrical rail vehicles. In many developing countries, the reliable access to electricity is still a big challenge and about 55.7% of Ethiopians still have no access to the national electric grid or any other significant electricity source according to published studies. Some of the population depend on dry-cell batteries, or off-grid electrical energy supply which does not cater enough for ancillary services or basic energy needs. On the other hand, a total number of 41 train vehicles operate daily on the two lines namely E-W line and N-S line of the AALRT and consume a huge amount of energy that is entirely drawn from the national grid. Part of this energy goes to the auxiliary power supply unit to feed some AC and DC loads onboard of rail vehicle such as those that are captious to its effective and safe operation. A portion of this energy could be saved and used to supply some of the Ethiopians who have no access to electricity at all.

This research proposes a strategy of onboard auxiliary supply system of light weight train using photovoltaic and battery energy storages. The structure proposed here is to install the solar panels on the train's roof with onboard batteries. Data were collected, and an in-depth analysis was performed to assess the possibility of supplying them using roof-top PV and battery storages in the case of AALRT. A demand-supply analysis was carried out in this study to compute the system availability and reliability. Accordingly, the PV system was optimally sized along with a battery control strategy. The study included details on MPPT algorithm, and energy management strategy of system.

Results of the study prove that a combination of PV system with existing onboard batteries can help to save 3.33MWh daily. It has been demonstrated that the system would return the investment within 20 months through the payback period approach. Shading analysis of the proposed PV system has also been carried out for two identified locations with potential shadow-cast building and it has shown that only 0.8% and 1.3% for case 1 and case 2, can be lost. This loss is negligible for since we considered the worst-case scenario. The availability of regenerative energy has also been briefly analyzed and the performance of the designed system has been evaluated.

Acknowledgement

First and foremost, I want to thank God for guiding me through this research. I would like to express my sincere gratitude to my advisor Mengesha Mamo (PhD) for his invaluable assistance and contributions to this research work. I value his breadth of knowledge and attention to detail, as well as the constant encouragement he has provided me throughout this research. I would also like to express my gratitude to the lecturers who assisted us throughout the two semesters of coursework. My heartfelt gratitude goes to the World Bank and all collaborators for their financial support of this research project. I also thank the AAIT and the ARCE administration for ensuring the well-being of its students. I would also like to thank my family for their prayers and support. My thanks also go to my friends and colleagues for their encouragements and contributions of any kind that helped in this research.

Dedication

This thesis is dedicated to my beloved family, my wife Diane, my daughter Chaxella, and my son Archie, who have been a constant source of support, motivation, and encouragement throughout my graduate school journey. I am so grateful to have you in my life. This work is also dedicated to my mother and aunt, who have always loved me unconditionally and whose examples have taught me to work hard for Things that I aspire to achieve.

Table of Contents

List of Figures

List of Tables

Acronyms and Abbreviations

AALRT	:	Addis Ababa Light Rail Transit
AC	:	Alternating Current
ANN	:	Artificial Neural Network
A-P	:	Angstrom-Prescott
APS	:	Auxiliary Power Supply
ARPS	:	Auxiliary Railway Power Supply
BMS	:	Battery Management System
CdTe	:	Cadmium Telluride
CIS	:	Copper Indium Diselenide
CRH	:	China Railway Highspeed
CSP	:	Concentrated Solar Power
CV	:	Constant Voltage
DC	:	Direct Current
DoD	:	Depth of Discharge
EMU	:	Electric Multiple Units
ESSs	:	Energy Storage Systems
E-W	:	East-West
FL	:	Fuzzy Logic
Hz	:	Hertz
IGBT	:	Insulated Gate Bipolar Transistor
IC	:	Incremental Conductance
KVA	:	Kilovolt -Ampere
kW	:	Kilo-Watt

kWh	:	Kilo-Watt-Hour
LF	:	Low-Frequency
Li-ion	:	Lithium-ion
LRT	:	Light Rail Transit
MF	:	Mediu-Frequency
MPPT	:	Maximum Power Point Tracking
NASA	:	National Aeronautics and Space Administration
NiCad	:	Nickel Cadmium
Ni-MH	:	Nickel-metal hydride
NMSA	:	National Meteorological Service Agency
N-S	:	North-South
OCS	:	Overhead Contact System
PB	:	Pay Back
PC	:	Personal Computer
PI	:	Proportional-Integral
PSO	:	Particle Swarm Optimization
PV	:	Photovoltaic
PWM	:	Pulse Width Modulation
SESs	:	Secondary Energy Sources
SoC	:	State of Charge
THD	:	Total Harmonic Distortion
TMS	:	Time Management System
TPSS	:	Traction Power Supply System

CHAPTER 1: INTRODUCTION

1.1 Background of the Study

Today, the global population is estimated at 7.3 billion people and it has been forecasted that this number will keep rising up to around 8.5 billion by 2030 [1]. Passenger and freight transport demand has seen a substantial increase around the world, and it will continue to rise in the vicinity of main urban areas, with unsustainable environmental consequences. The current transportation model in all its forms is, without a doubt, unsustainable. Any increase in mobility implies serious pollution issues as well as increased energy demand, which, combined with a scarcity of natural resources, projects a dark future.

From an economic and environmental point of view, research towards the development of alternative energy options for the transportation industry is deemed indispensable. Over the last two decades, significant efforts have been made and continue to be made, not only in terms of technology, but also in terms of regulation, to reduce the adverse impact of transportation and promote sustainable development. For a variety of reasons, urban railway systems play a vital role in the long-term development of cities, the most significant of that is their relatively low power consumption to transport capacity ratio. Despite this, substantial improvements in energy efficiency are required to maintain their clear advantages above all other forms of transport in a world dominated by rising capacity demands and electricity bills [2].

The increased attention in the utilization of energy storage technologies to enhance the functioning of tramways has triggered evolving verification methods and excellent energy storage units in order to glean profits and lower the cost of installation [3]. Recently, the quick expansion of photovoltaic energy as renewables has also fueled the substantial interest in coupling renewable energy and storage units. Solar PV panels installation on rooftops of the current trains has established to become one of the many feasible significant green technologies for urban trains [4]. Maintaining high-quality and secure electrical utility services while attempting to rapidly decarbonize electric power systems is a significant challenge for countries all over the world. While renewable energy provides a cleaner and less expensive energy source, it is critical to assess the potential application of solar energy systems with storages which may produce sufficient electrical energy for the auxiliary AC and DC loads of electrical locomotives [5]. Railway onboard auxiliary systems are required for proper vehicle operation (fan engines, compressors, etc.), and

for passenger comfort or load conservation. These systems were previously limited, however, a growth in comfy needs onboard has resulted in an increase in demand.

Researches show that batteries, flywheels and supercapacitors are the three main storage technologies used in railway [6]. In the railway industry, traction energy consumption keeps rising and it is believed that railway auxiliary loads could be powered by track-connected solar which is not only cheaper but also low carbon than utility grid energy [7]. Electric railway lines present significant novel market businesses and opportunities that could unfold fresh commercial development of solar energy technology in Africa and beyond [7].

1.2 Problem Statement

Climate change continues to affect the world, and alternative energy sources are being studied extensively. There is an urgent need to reduce carbon emissions in public transport and railway systems should not be left behind in this transformation. When compared to conventional sources, renewable energy produces 750 grams of CO2 less per kWh [8]. Furthermore, in many developing countries, the reliable access to electricity is still a big challenge and about 55.7% of Ethiopians still have no access to the national electric grid or any other significant electricity source according to [9], [10]. Some of the population depend on dry-cell batteries, or off-grid electrical energy supply which does not cater enough for ancillary services or basic energy needs. A total number of 41 train vehicles operate daily on the two lines namely E-W line and N-S line of the AALRT and consume a huge amount of energy that is entirely drawn from the nation grid. Part of this energy goes to the auxiliary power supply unit to feed some AC and DC devices on locomotives, such as those vital to the train's protection and functionality. Other equipment such as air compressor, door control system, cooling fans, air conditioners, air dryer, communication system, charger and battery pack, electric lamps etc. are also fed from this auxiliary power supply unit. We believe that some of this energy could be saved. Furthermore, power fluctuations from the overhead contact system (OCS) usually causes communication failures which lead to delays and discomfort of passengers due to sudden stops.

Ethiopia is geographically located in the equatorial region where the sun is almost perpendicular throughout the year. Therefore, the country has sufficient daylight with more than 340 sunshine days and can potentially produce 4.5 to 7.3kWh/m2/day. This research thesis proposes an effective

design of secondary energy sources (SESs) consisting of photovoltaic and battery storages to supply the onboard auxiliary load of light weight train.

1.3 Research Questions

1. What are the technical requirements and application situation of the AALRT and its auxiliary system supply?
2. Are the auxiliary loads (Air Conditioner) optimal in the Addis Ababa environment?
3. What are the benefits to operate solar powered auxiliary loads on train vehicles?
4. How are the parameters such ambient temperature, incident solar radiation impacts the performance of the designed system?
5. Is the energy generated from the roof-top PV and onboard batteries enough to cater for all auxiliary loads?

1.4 Objective

1.4.1 General Objective

The general objective of this thesis is to propose an effective computer model of Photovoltaic and energy storage for auxiliary loads of light weight train; case of Addis Ababa Light Rail Transit (AALRT).

1.4.2 Specific Objectives

i. To collect data and analyze the auxiliary loads energy requirements and the possibility of supplying them using roof-top PV and battery storages in the case of AALRT.
ii. To compute the effective area and optimally size the PV and the battery energy storage for the onboard auxiliary loads.
iii. To design an effective computer model of the PV and Battery storage and perform the shading analysis of the array.
iv. To evaluate the performance of the designed system.

1.5 Significance of the Study

Climate change continues to cause havoc around the world, and alternative energy sources are being thoroughly investigated. There is an urgent need to reduce carbon emissions in public transport and railway systems should not be left behind in this transformation.

The major significances of this study are basically to inform the Ethiopian Railway Corporation about the possibility of supplying some auxiliary loads with renewables and save energy. The study also provides a general information on solar resources potentials of Ethiopia and ways of harnessing it to increase the potential use of alternative energy. The study further encourages the Ethiopian Railway Corporation to participate in the reduction of global warming by promoting renewables.

1.6 Scope of the Study

This research merely focuses on designing an effective system of secondary energy sources for onboard auxiliary loads of light weight train. It carries out an analysis of the proposed system topology and its control strategy for a better performance. The scope of this research is limited to analyzing the impact of PV and battery storage system on the auxiliary power supply unit and it does not discuss the details of the aerodynamic and boundary condition effect of the moving air at the top surface. The study looked the availability of regenerative braking energy for supplying other high power ac loads. However, it does not provide a detailed analysis on the connection and conversion for this energy.

1.7 Thesis Organization

The thesis is divided into five chapters, which are as follows:

Chapter 1 of the thesis is the introduction. It describes the research's background, the problem statement, and presents the goals of the study in terms of General and Specific Objectives.

Chapter 2 provides a review of the current literature in this field of study. It describes the various topologies and operating principles of auxiliary power supply systems. It provides an overview of photovoltaic technologies, as well as charge controllers. Finally, this chapter discusses some related works as well as research gaps that have been identified.

Chapter 3 presents the methodology and procedures used to achieve the objectives described in Chapter 1. It entails system design, modeling, and data collection. It provides a thorough methodology for system evaluation and shadow analysis.

Chapter 4 provides a detailed analysis and discussion of the study's findings in relation to the objectives and methodologies described in the previous chapters.

The conclusion, research limitations, and recommendations are presented in Chapter 5.

CHAPTER 2: LITERATURE REVIEW

2.1 Auxiliary Power Supply System

The Electric Multiple Units (EMU) technology in any electric train integrates several sophisticated systems, and one of the key parts of the EMU is the auxiliary power supply system. The auxiliary supply system not only powers all load devices that require power except the traction power system, but it also guarantees the stable functioning of some parts of the EMU, ensuring people's lives and safe travel. It provides detached alternating current and direct current voltages for critical power loads in locomotives. DC-DC converters for APS are required to isolate the APS from the catenary voltage and to create a stable voltage for output converters [11]. The effective functioning of the auxiliary power supply system is required to ensure the stable and safe operation of the electric train. Auxiliary converters, chargers, batteries, and related loads are the main components of the EMU auxiliary power supply system. A simplified schematic illustration of a standard APS system for 750 VDC and 1500 VDC catenary voltages is shown in figure 2.1 [11], [12].

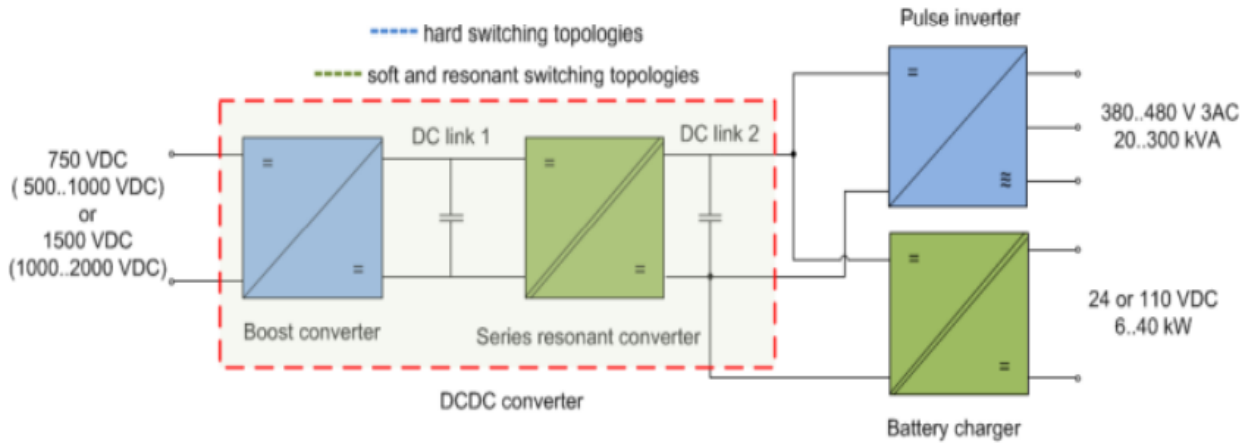

Figure 2. 1: Standard APS System for 750 VDC and 1500 VDC Catenary Voltage [11].

The voltage from overhead contact system has a broad range (such as 1000 to 2000 VDC for a catenary voltage of 1500 VDC). Transient voltages must also be considered in the converter design. Power semiconductors with voltage ratings of 1200 V or 1700 V are commonly used. As a result, series connections are commonly used. Typically, a parallel connection is used for power expansion. In addition, passive components such as transformers and chokes are essential to the design. The DC-DC converter becomes complex as a result of this and the requirements for railway applications, and it has a significant impact on the overall APS design.

2.1.1 Indicators of Performance Assessment

The train's auxiliary power supply system's optimization or performance can be evaluated using a variety of methods so as to accurately guarantee the APS's design quality, minimize system faulty, and increase design optimization. When the APS of an electric train is optimally configured, performance evaluation indicators such as system dependability, economic environment, convenience, and environmental impact improve. APS system steadiness, fault tolerance configuration and natural ecosystem resilience are all examples of reliability. The price is an economic indicator; the comfort and lighting systems are comfort indicators; and the system's energy quality and environmental impact are environmental indicators [13].

2.1.2 ARPS Descriptions and Current Architectures

The voltages of European dc standard catenaries can range from 600 to 3 kV. The ARPS is a transitional electric process that converts the voltage from the overhead contact system to the voltage levels suitable for onboard auxiliary systems of locomotives. The interface requirements between the loads and the inverter must be established jointly by both the locomotive and static converter manufacturers, according to current regulations. When it comes to the maximum allowable THD, it turns into tradeoff between the expenses of the inverter output filter, sophistication, and dependability and the expense and robustness implications. Customers can also request specific requirements.

It could, for example, be ordered to design bidirectional feeding of the auxiliary systems for the purpose of powering them from an exterior 400 Vac source at the garage while leaving the inverter turned off [14]. Table 2.1 summarizes a set of common ARPS specifications, as well as frequently used THD benchmarks.

Table 2. 1: ARPS Regular Specifications[14]

Parameter	**Range**
High DC input voltage	600V to 3KV
Three phase AC output	400 Vac (line to line)
Maximum THD @ AC output voltage	<4%, <7%, <14%
DC output Voltage	24 Vdc, 72 Vdc, 100 Vdc
Galvanic Isolation	Input -Output
	AC Output-DC Output

Historically, the ARPS has been implemented in accordance with the scheme depicted in Figure 2.3. The low-frequency (LF) transformer, on the other hand, suffers from shape and high volume owing to its limited operating frequency: 50/60 Hz [15].

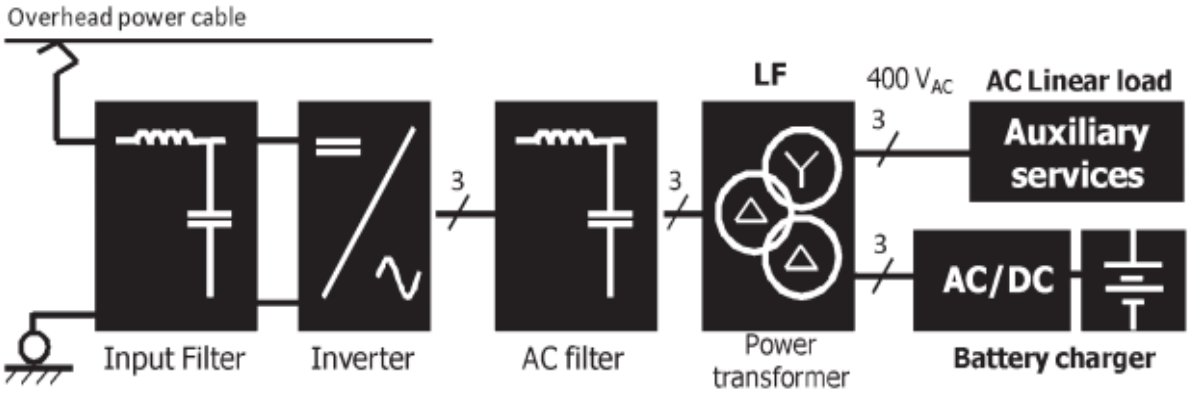

Figure 2. 2: Schematic View of a standard Metro APS with LF Transformer [14]

In terms of power electronics options, a new technology layout has been introduced in recent years as a means to lower transformer weight and volume. The structure depicted in Figure 2.4, is built around a transitional conversion phase that employs medium-frequency transformers.

Even though MF transformer solutions substantially reduce transformer weight and volume, when particularly in comparison to LF transformer solutions, switching losses upsurge and reliability declines; this is particularly true for high-voltage catenaries. As a result, the LF topology is recommended for HV catenaries because it is economical, reliable, efficacious, and widely applied.

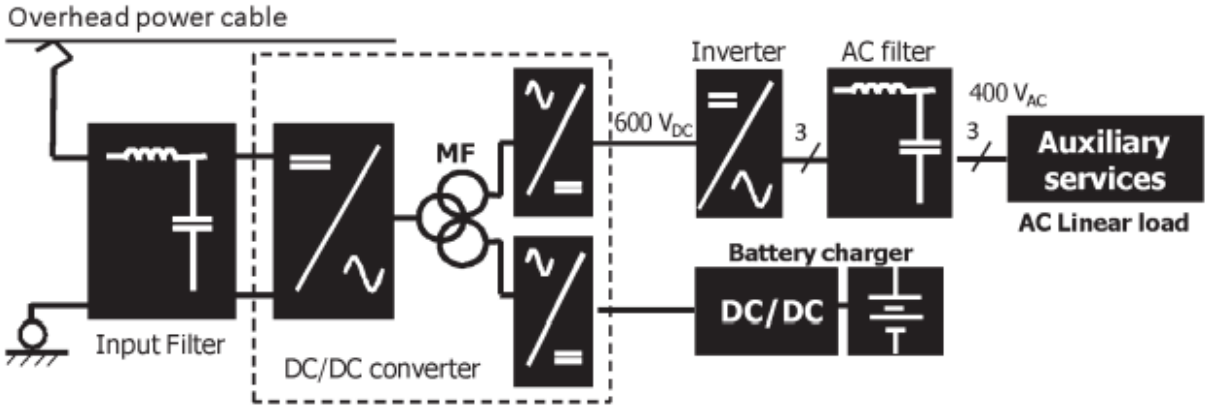

Figure 2. 3: Schematic View of a standard Metro APS with MF Transformer [14]

Table 2.2 summarizes a comparison of the two technology layouts in terms of benefits and limitations.

Table 2. 2: Comparison of ARPS technology layouts from DC Catenaries [14].

Transformer type	Benefits	Limitations
LF Transformer	• Less expensive • Robustness • High Reliability • High Efficiency • Better EMI	• Heavy Weight • Size of the Transformer
MF Transformer	• Weight • Size Reduction of the Transformer	• Number of stages • Number of semiconductors • Low Reliability • Increased switching frequency • Increased switching losses especially in HV catenaries

2.1.3 Addis Ababa Light Rail Transit Auxiliary Power Supply System

In the case of AALRT, APS system includes auxiliary inverter and batteries. The auxiliary inverter provides AC380V and DC24V to onboard auxiliary loads while also charging the batteries. If a high input voltage of DC 750V is unavailable (auxiliary inverter faulty), it also provides control power and a case of emergencies power supply to vehicles. The auxiliary inverter, figure 2.5, mainly consists of line contactor group, IGBT inverter power unit, 3-phase isolation transformer, logic control unit and filter capacitor. It converts 750 VDC to 3-phase 380 VAC (with a N line for supplying 220 VAC), which is then fed to onboard auxiliary equipment. Similarly, It will also step 750 VDC down to 24 VDC, which will be used as the control electrical supply for the whole onboard control systems and loads.

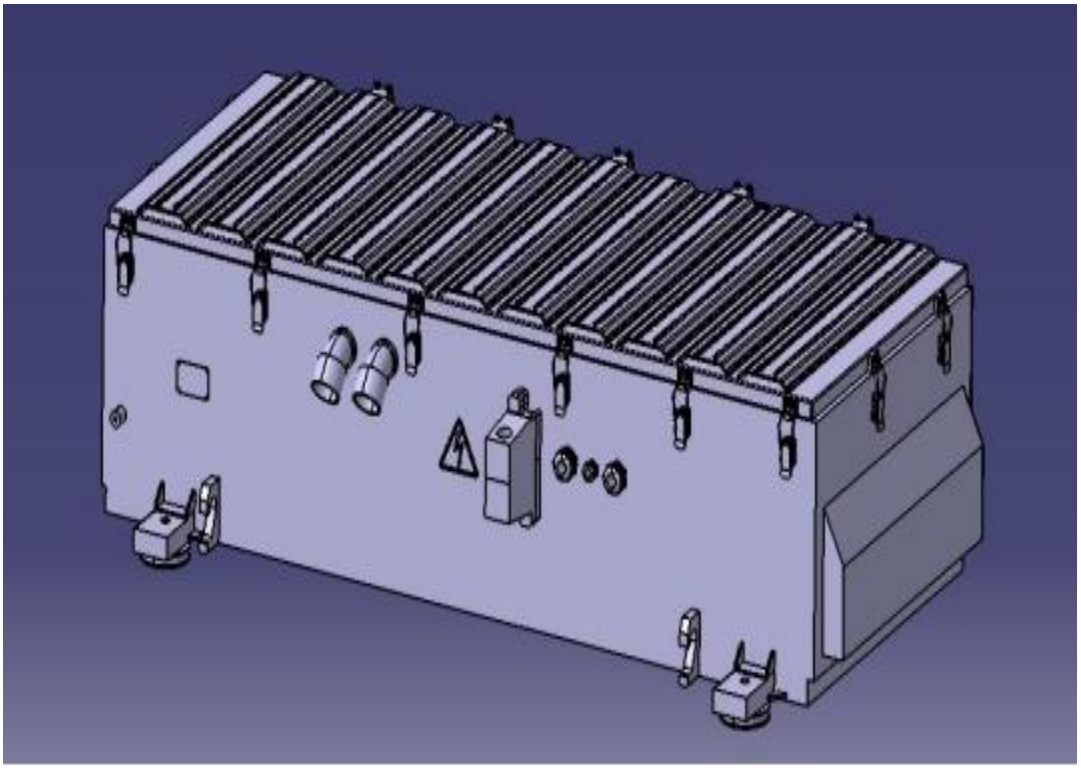

Figure 2. 4: Auxiliary Inverter of the AALRT

The APS involves an auxiliary inverter control module for output of the APS system's logic control signal, to manage the operational activities of the auxiliary inverters and charger, to react to all controlling instructions, and to implement APS-controlled functions tailored to specific features. For external communication, it is connected to the controlling unit of the vehicle via CANOpen. It is linked to a local PC or flexible unit via serial ports for data and instruction downloads, audio, and web adapter implementation. There are totally two APSs across the train. Auxiliary power supplies are directly wired in parallel. Each APS system can directly transfer power to the train's AC bus and provide 380VAC auxiliary power across the train locomotive. If one of the auxiliary inverters fails during operation, it will instantaneously disconnect the auxiliary inverter's output contactor and separate the AC vehicle bus from that auxiliary inverter. AC equipment on the vehicle will be fed by the remaining auxiliary inverter via the vehicle's AC bus. In this case, a faulty auxiliary inverter will generate a failure signal, and onboard auxiliary equipment on will have degraded functions via TMS.

2.2 Photovoltaic Technologies and Solar Energy Resources

In recent decades, solar power has gained popularity as a result of technological advancements as well as government policies that promote the production and application of green energy sources. It has undergone a significant technological transformation. Despite the use of limited scale photovoltaic cells in the early stages of solar technologies, solar concentrated power (CSP) and massive PV systems that supply power electricity grids are prevalent nowadays. Solar system technologies come in a different patterns, sizes, and configurations, and types.

a. Monocrystalline Silicon Solar Panels

Such type of panels is made up of cells that have been cut from a single silicon cylindrical crystal. This is the most energy-efficient photovoltaic technology, turning approximately 15% of the sun's radiation into electricity. Monocrystalline silicon necessitates a more complicated production line, resulting in moderately increased costs than most other solar technologies.

b. Polycrystalline Silicon Solar Panels

Polycrystalline silicon cells, also referred to as multicrystalline cells, are created by extracting cells from a melted and recrystallized silicon ingot. After that, the ingots are cut into quite thin slices, that are then arranged into whole cells. Because of the easier production process, they are typically less expensive to produce compared to monocrystalline cells, but they are slightly less effective, with an average efficiency of around 12%.

c. Thick-film Silicon Solar Panels

This one is also a multicrystalline innovation in which silicon is steadily placed onto a base material, producing a fine-grained, good appearance. As with all crystalline PV, it is usually embedded in a transparent insulating polymer with a heat - treated glass cover before being bound into a steel package.

d. Amorphous Silicon Solar Panels

Rather than making a stiff crystal layer, amorphous silicon cells are made by depositing silicon in a slender homogeneous layer onto a substrate. Since amorphous silicon refracts light more efficiently than crystalline silicon, the cells can be made slimmer, earning it the nickname "thin film" PV.

Amorphous silicon can be dumped on a variety of hard and soft substrates, making it suitable for curved surfaces or direct bond formation to roofing materials. This particular technology is less effective than crystalline silicon, with average efficiencies of about 6%, but it is simpler and less expensive to manufacture. An amorphous substance may be a good choice if roof space is not a concern. Specifiers should choose crystalline technology if maximum performance per square meter is needed.

e. Other Thin film PV Panels

PV modules are now made of other varieties of materials, including cadmium telluride (CdTe) and copper indium diselenide (CIS). These technologies are enticing because they can be implemented using relatively low-cost industrial operations, especially when compared to crystalline silicon technologies, and they typically have higher module efficiencies than amorphous silicon. Most are slightly less effective: CIS is normally 10-13 percent efficient, while CdTe is about 8 or 9 percent efficient. Although a standard CdTe module contains just 0.1 percent Cadmium, which is approximated to be less than what is comprised a single AA-sized NiCad battery, the use of highly toxic metals such as Cadmium and the need for both closely regulated production and end-of-life disposal are disadvantages.

A comparison of various solar photovoltaic panel types can be found in table 2.3 bellow.

Table 2. 3: Solar PV Technologies Comparison [16]

Property	Monocrystalline	Polycrystalline	Thin Film, Amorphous Crystalline etc.
Efficiency	High	Reasonable (13-15%)	Low
Cost rate	High	Reasonable	Low
Density	Low	Reasonable	High
High Temp. Performance	Weak	Weak	Good
Generation in diffused light	Medium	Medium	Good

2.2.1 PV Systems and Charge Controllers

In recent years, the PV technology development and generation has been increasing at a galloping rate around the world. The progressive technological upgrading of enterprises and the optimization of the PV market are the main factors behind the global energy transformation for more renewable energy consumption [3], [17]. The technological innovation and advancements of PV generation sector is expected to continue to drive industrial upgrading along with the conception of quality photovoltaic cells. This has been the case, year by year and rapid progress in the conversion efficiency of PV panels is being achieved. Photovoltaic panels generate current at a specific voltage that is proportional to the amount of solar radiation that strikes the panels' cells [18].

The electrical circuit diagram of solar PV module is illustrated in Figure 2.6 The current I at the output terminals is represented by the subtraction of the diode current I_d and the shunt current I_{sh} from the generated light current I_l. Rs which is the series resistance symbolize the internal resistance of the current flow. It is a function of the pn junction depth, electrical impurities, and resistance. The shunt resistance R_{sh} is pertaining to the leakage resistance into ground [5].

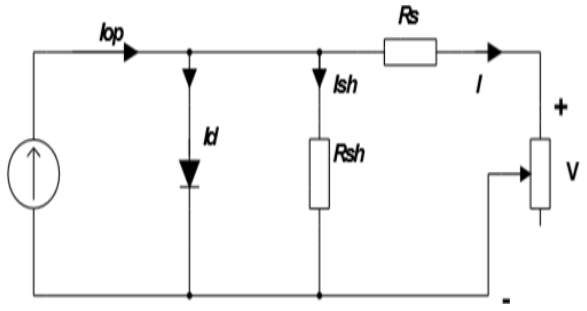

Figure 2. 5: Electrical Circuit Diagram of Solar PV Module

$$R_{pv} = -M\frac{I_{sc}}{I_{MPP}} + \frac{V_{MPP}}{I_{MPP}}\left(1 - \frac{I_{sc}}{I_{MPP}}\right),$$

$$V_T = -\left(M + R_{pv}\right)I_{sc}, \tag{1}$$

$$I_0 = I_{sc}\, e^{\frac{V_{oc}}{V_T}},$$

$$I_{ph} = I_{sc}.$$

where R_{pv} is the PV resistor; I_{ph} is the photon current; I_{sc} is the short circuit current; I_{MPP} is the current at maximum power point; V_{MPP} is the voltage at maximum power point; V_{oc} is the open circuit voltage.

The gradient M is required for the calculation. It is a function of the following parameters:

$$M = f(V_{oc}, \quad I_{sc}, \quad V_{MPP}, \quad I_{MPP}) \tag{2}$$

The following approximation of the characteristic curve can be derived with an accuracy of 1%.

$$M = \frac{V_{oc}}{I_{sc}}\left(K_1 \frac{I_{MPP}\, V_{MPP}}{I_{sc}\, V_{oc}} + K_2 \frac{V_{MPP}}{V_{oc}} + K_3 \frac{I_{MPP}}{I_{sc}} + K_4\right) \tag{3}$$

With the equation constants:

$$K_1 = -5.411$$

$$K_2 = 6.450$$

$$K_3 = 3.417$$

$$K_4 = -4.422$$

When the sun is not available, the electrical energy should be stored, generally in battery packs. Photovoltaic modules basically have a particular I-V curve that changes with ambient temperature and the rate of sunlight or the angle at which the sun hits the modules [18], [19]. Rising temperatures reduce voltage, while increased sunlight tends to increase output current. Loads, however, have voltage level and current level requirements that are independent of, and frequently differ from, what the PV panel generates. To address this mismatch, a charge controller device is interfaced between the panels and the battery packs or load. Primitive charge controllers could only help decrease the photovoltaic panels voltage if it was too high for the battery packs. Advanced and more effective charge controllers have cropped up, allowing for a better match between PV systems and loads. Their primary purpose is to get all of the power generated by the PV panels, irrespective of voltage and current, at any level of solar insolation or temperature.

2.2.2 Photovoltaic Maximum Power Point Tracking Systems

Photovoltaic has been one of the advanced technologies that uses the photovoltaic effect to transform solar radiation directly into electrical energy. To improve the efficiency of PV modules, a lot of research has been done. The solar PV generating panels, on the other hand, have two major flaws. First, solar PV cells have a low conversion efficiency (9% to 17%), particularly in limited irradiation settings. Second, the total amount of electricity generated by solar PV panels fluctuates constantly depending on atmospheric conditions. Furthermore, the I-V curve of the solar cell is non-linear and fluctuates with irradiance and temperature [20]. On the I-V or P-V curve, there is usually a single point known as the Maximum Power Point. As a result, the solar PV system will become as effective as possible and provide the maximum amount of power.

To overcome the efficiency restriction, several methods for monitoring a Photovoltaic module's maximum power point have been developed. A MPPT is a process of collecting and supplying the maximum amount of power from a solar PV panel to the load. It is an electrical DC to DC converter that enhances the solar arrays (PV panels) and load compatibility. It regulates the operation of photovoltaic (PV) modules to guarantee that they generate the maximum amount of power possible [21], [22]. Although the MPP is not evident on the I-V or P-V curves, it can be found using search techniques like the Perturb and Observe algorithms [23], [24], the Incremental Conductance (IC) algorithm [25], the Constant Voltage (CV) algorithm [26], the Artificial Neural Network (ANN) algorithm [27], the Fuzzy Logic (FL) algorithm [27], the Particle Swarm Optimization (PSO) algorithm [28]

Of these, it is straightforward to see that the traditional P&O algorithm is among the most basic MPPT methods. It has a basic construction, is easy to install, is less impacted by the solar PV panels' intrinsic capacitance and has a desirable flexibility to slowly fluctuating solar irradiation and temperature circumstances and it has been implemented in this research thesis.

2.3 Energy Storage Techniques in Railway Electrification Systems

Over the recent few years, electrical industries have continued to implement new electricity production technologies to respond to the ever-increasing demand. Considerable studies have been conducted focusing on renewable energy sources in order to address the issue of global warming and climate change. Unfortunately, the sporadic characteristic of renewable sources of energy reduces their effectiveness. Furthermore, energy storage systems are regarded as the most

important component of electric vehicles. As a result, effective and appropriate methods of storing the energy generated for future use when the solar radiation is unavailable, and the wind is not blowing have been developed. In recent decades, energy storage techniques have advanced and adjusted to newer energy needs and availability. Today, there is a wide range of energy storage choices available for a variety of applications. Numerous metrics are used to classify these energy storage systems, such as reaction time (energy storage or electric power storage), appropriate storage period (brief, intermediate, long-term), and scale (small, medium, large-scale) [29]. Furthermore, the various energy storage technologies have been subdivided based on the form in which they are stored. in figure 2.7.

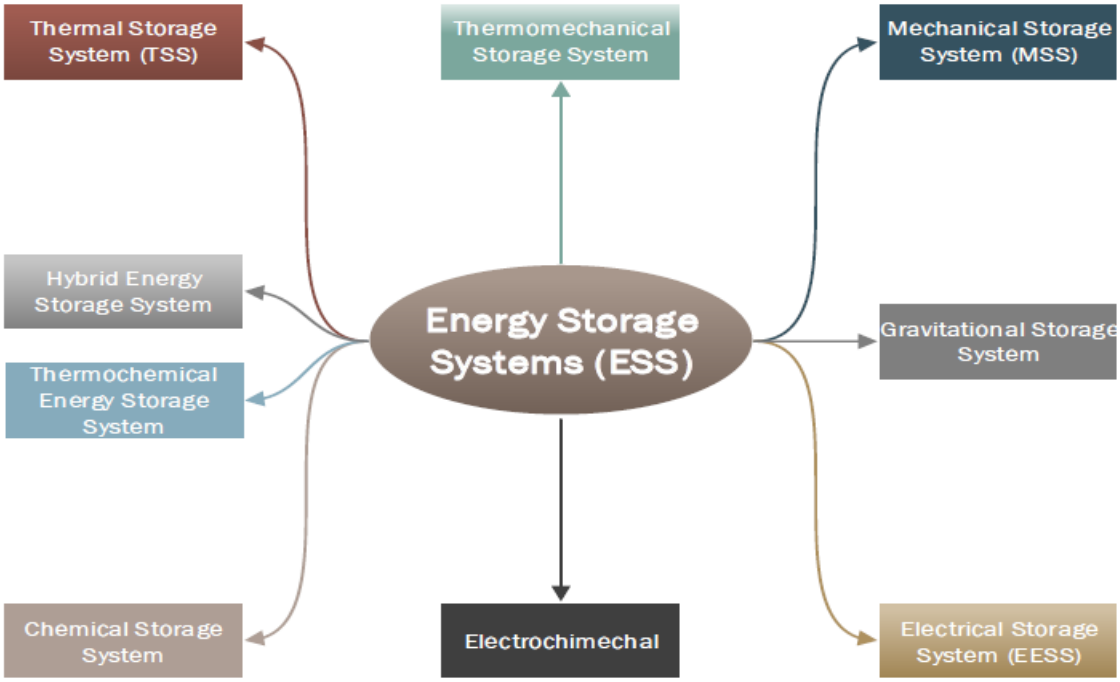

Figure 2. 6: Energy Storage Systems Classification

2.3.1 Batteries

The battery is the traditional and most frequently utilized electric energy storage technology. A battery is composed of many electrochemical cells wired both in series and parallel to form a single unit. Two electrodes are submerged in an electrolyte solution to form cells. Batteries operate on the basis of the following scheme: reversible chemical processes occur at the electrodes, causing

a potentiometer to charge and discharge. As a result, energy can be converted from electrical to chemical form in a reversible manner [2], [30]. It is a secondary electric generator, which means that it cannot function unless it has previously been supplied with electricity, which is known as charging.

Based on the electrode and electrolyte materials, many types of batteries exist. Lead–acid, lithium–ion, nickel–metal hydride, and sodium sulfur are the most prevalent types utilized in rail transit systems (Na-s). Other different battery types, such as flow batteries, could be employed in rail transport systems [31]. Table 2.3 summarizes a comparative analysis of the benefits and drawbacks of each type [32].

Table 2. 4: Various Battery Storage Technologies Comparison

Bat. Type	Strengths	Weaknesses	Remark	Reference
Pbso4	• Low cost/Wh • Long history • Wide deployment • High reliability • High power density	• Less cycles • Limited charging current • Limited life cycle • Environmental issues • Weak performance in low temp.	Substantial investigations have recently been conducted on the substitution of lead with some other components such as carbon in effort to expand power and energy density.	[2], [33]
Ni-MH	• Long life cycle • High density • High Ch./Disch. current • Less environmental concern	• Higher cost per Wh • Frequent maintenance • Higher-self disch. rate	The main concern of high self-discharge can be mitigated through using new separators.	[2], [34], [35]
Li-ion	• High En. density • Small and light • Less mainten. • High no. of cycles	• High cost per Wh • Cell balance and control to avoid overcharge. • Special pack and protect.	Currently researchers are investigating a mixture of electrochemical and mono-structures that can help enhance Li-ion batteries	[2], [36]
Na-s	• High En. density • High P. density • High Ene. effic.	• Increased cost • Environmental concern • Need cooling system	Scientists are looking into innovative ways to lower their high working temperatures.	[2], [33], [36]

ESS can be used in two settings: onboard and at the roadside. The storage material is mounted on the vehicle in onboard ESS. It can be mounted on the vehicle's roof or under the floor. Because room is limited, it is relatively costly to install ESS beneath the floor. Onboard ESS efficiency is strongly reliant on vehicle characteristics, which can have a direct impact on the amount of electricity generated and used through braking and acceleration, respectively. Other advantages of onboard energy storage include peak power shaving, voltage regulation, operation without catenary, and loss minimization [32].

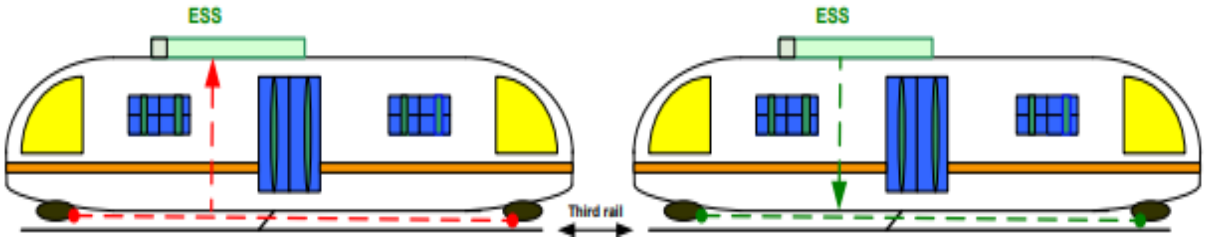

Figure 2. 7: Onboard Energy Storages Systems

2.4 Related Works

In an effort to minimize the load on the utility grid, an efficient solar system energy integration was proposed in [8], [37], [38]. The proposed scheme makes use of an advanced combination of electricity produced by solar panels mounted on an external existing surface and grid power. The battery banks are placed on each of the two sides of the traction bridge support pillars. Power flow analysis and design has been performed to understand the system. A technical strategy for a passenger train's APS centered on photovoltaics and battery storage has been introduced in [39]. The topology structure of system includes solar photovoltaic panels, DC-DC converter along with a specific MPPT algorithmic program, a DC-DC converter with bi-direction configuration, battery packs for storing energy, and a smart battery management system referred to as BMS. Its operation considers the panels output power linked with a DC-DC converter, that helps to raise the voltage rate and keep tracking the output at maximum power point. The battery banks are linked by a bi-directional DC-DC converter, which is able to obey to instructions from the Energy Management System referred to as EMS and then regulate or manage the action of charging or discharging of the batteries. Finally, the paper estimates the year's electricity production capacity and analyzes

system performance, the impact of conserving energy, and carbon diminution. Wu Mingliang *et al,* proposed a back-to-back solar energy generation technology and control mechanism for electrified railways [15]. Solar electric energy is provided by a DC link capacitor of a back-to-back converter in the developed framework. The overlapping potential of the converters is being used to achieve TPSS reactive power and NS or negative sequence current compensation. The solar panels output power as well as the rated capacity of the converters are taken into account in the optimization process. MATLAB/Simulink was used to model the traction power supply system referred to as TPSS and the S-Function was used to implement the control scheme. In reference [40], the authors introduced a scheme for photovoltaic solar incorporation on rooftops of train cars is being considered for South African Railway industry. The study was motivated by the average growth in freight transport demand, which resulted in high costs associated with annual Traction Substation upgrades to meet the requirement. According to the authors, because of the high demand for freight transport, high train congestion causes traction substations to overload. The primary goal was not to completely replace conventional electric energy generation, but rather to embed a solar photovoltaic system as an additional energy supply to minimize traction Substation overloading, thereby improving energy efficiency and hauling more cargoes to respond to the demand and adjusting to Transnet Freight Rail's Market Growth Policy of being regarded as the five largest freight company in the world [41]. The work reported in [19], creates a solar based electric energy generation system on the ceiling of Gwangmyeong Station, Korea's biggest railway station building, and uses PVsyst to compute expected energy generation volume. Finally, the article sought to determine the influence of solar power generation systems on greenhouse gas emission minimization in electrical railway transportation networks. Another important contribution is reported in [42], [43] where a consideration is given to supplying electricity from a solar photovoltaic system placed near the equipment box and a wind energy, which is interconnected with the utility grid and utility grid network supplies power to railcars on the traction line via their substation. To test the performance parameters of both systems, the response of the traction power supply system was evaluated through simulation.

CHAPTER 3: DESIGN AND MODELLING

This section of the research portrays the methodological approaches and procedures that are utilized in order to accomplish the goals of the study. It is worth noting that the aim of this research is not to entirely eliminate the conventional energy supply for light rail trains but to alternatively propose an integration of a roof-top solar photovoltaic and onboard energy storages for auxiliary loads, therefore reducing the power drawn from the utility grid. An efficient integration scheme of PV and ESSs is developed for the auxiliary loads in case of Addis Ababa Light Rail Transit (AALRT). The simulations are performed using Google Earth, PVSyst and MATLAB.

3.1 PV Array Design and Modelling

Solar photovoltaic electricity is created by converting photons into electric power through semiconductor devices or materials. Photovoltaic generators are made up of many solar cells where this solar cell is the key component which can only deliver a limited power in terms of few watts. Furthermore, in order to get higher amount of power for extensive electrical energy installations, it is necessary to connect numerous solar panels both in parallel and/or series, which is commonly known as solar PV array.

Photovoltaic panels generate current at a specific voltage based on the amount of solar radiation that strikes the panel's cells.

In this work, the roof top of the train car surface area is a fixed parameter in the calculation and design of the PV array. The solar panels, which are composed of solar cells linked in a specific pattern, cover a specific region of the roof top of the train cars. Figure 3.1 gives a schematic representation with detailed dimensions of the vehicle to be considered throughout the design.

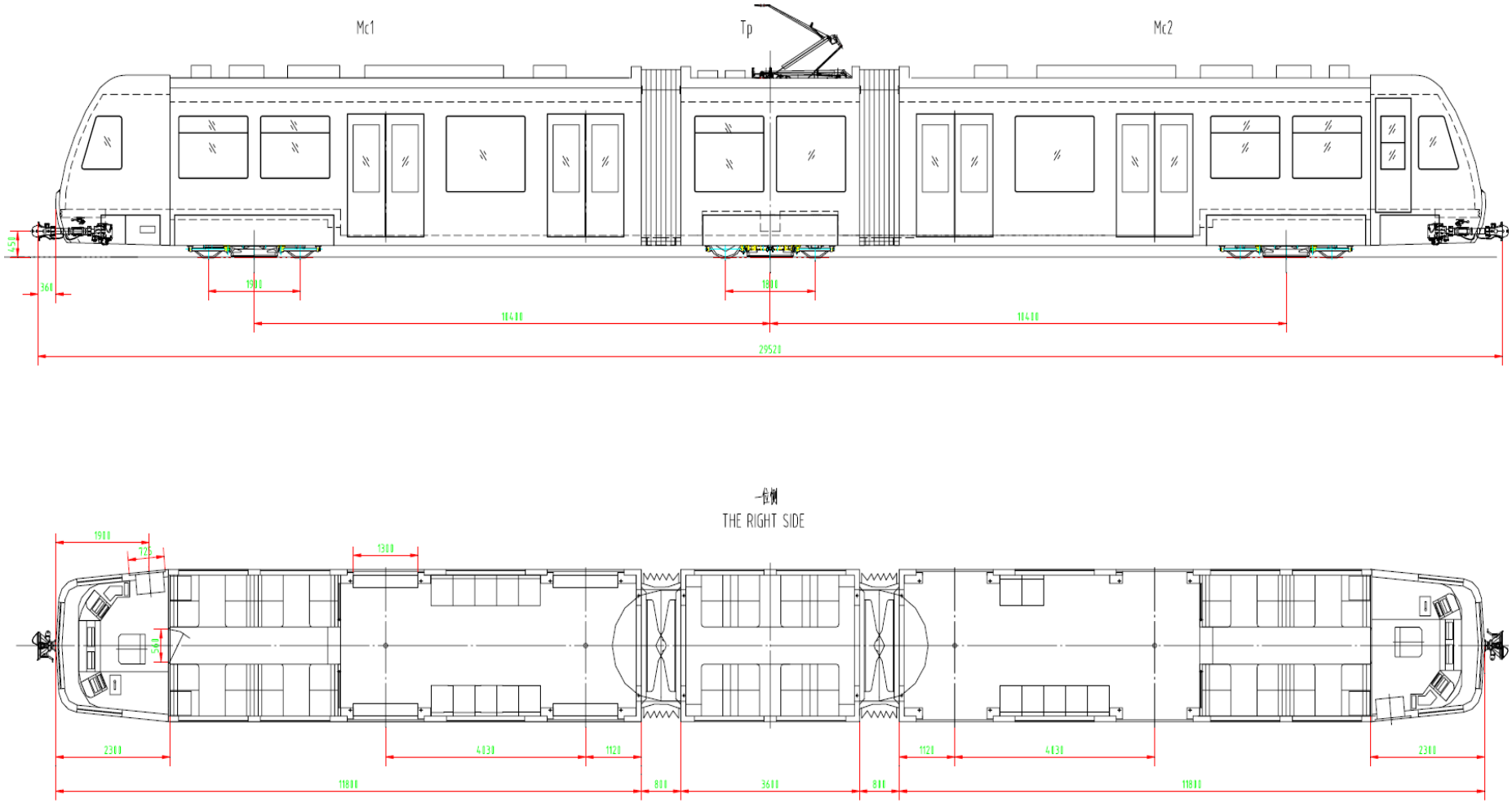

Figure 3. 1: Train Dimensions

Table 3. 1:Train Specifications at AALR

No.	Parameter	Value
1	Train car weigh	44tone
2	Vehicle Car weight with full passenger 6persons/m^2	59.24tone
3	Height of the vehicle (excluding pantograph)	3.7m
4	Vehicle length (single vehicle)	29.4m
5	Car body width	2.65m
6	Maximum operation speed	70km/hr
7	Operation base speed	40km/hr
8	Acceleration under rated load (from 0-40km/hr)	1m/s^2
9	Acceleration under rated load (from 0-70km/hr)	0.5m/s^2

3.1.1 Effective Area Calculation and PV Array Sizing

The total area of the roof of an AALRT train car that operates on either line (E-W or N-S) can be calculated based on its dimension reported both in table 3.1 and figure 3.1.

$$A_T = 29.4m \times 2.65m = \mathbf{77.91\ m^2} \quad (4)$$

Where A_T is the total area of the roof.

Different solar cell technologies have been developed in past few decades and a considerable range of them is already available in the market. In this study, for the purpose of optimizing the available area, a monocrystalline solar cell technology has been considered. Because a single solar cell cannot generate much electricity, they are clustered together in solar panel modules. A solar panel's number of cells can range from 36 to 144 cells. 60-cell and 72-cell solar panels are the two most common solar panel types on the market today.

Solar panels with 72 cells have more photovoltaic cells and are thus larger than panels with 60 cells. 60-cell panels are normally six cells wide and 10 cells tall when it comes to dimensions. Sixty-cell panels are also six cells wide, but 72-cell panels feature two additional rows of cells,

making them slightly taller. As a result, 60-cell solar panels have an average size of 5.4 ft by 3.25 ft. The 72-cell panels will have nearly the same width with an average height of 6.5 feet. When it comes to solar system design, this extra area can make a major difference. 60-cell panels, on the other hand, are advised for fitting in more tight locations if there is a limited room for installation or if the arrangement is more sophisticated, as in our case. Therefore, a 320W monocrystalline module (**OSMp60-320W, 1689mm×992mm)** composed of 60 squares or individual cells linked to each other by wires has been considered in this study. Its specifications and dimensions are reported in the datasheet of figure 3.2 bellow. The electricity is carried by the cables to a junction where the panel is connected to a large array.

The area of one panel is then given by:

$$A_P = 1.689m \times 0.992m = \mathbf{1.675\ m^2} \quad (5)$$

Where A_P is the panel area.

Considering the highest possible distribution of the PV modules on the ceiling, as shown in figure 3.2, taking into account that the total area of the roof is not entirely for PV installation due to equipment such as the pantograph spot, circuit brakers, spacing between modules, walkway, fixing access, and other equipment, the roof can accommodate up to 32 PV modules, 16 in longitudinal orientation (16 x 1.65m = 26.4m<29.4m) and 2 modules transversal orientation (0.992 m x 2 = 1.984 m < 2.65 m).

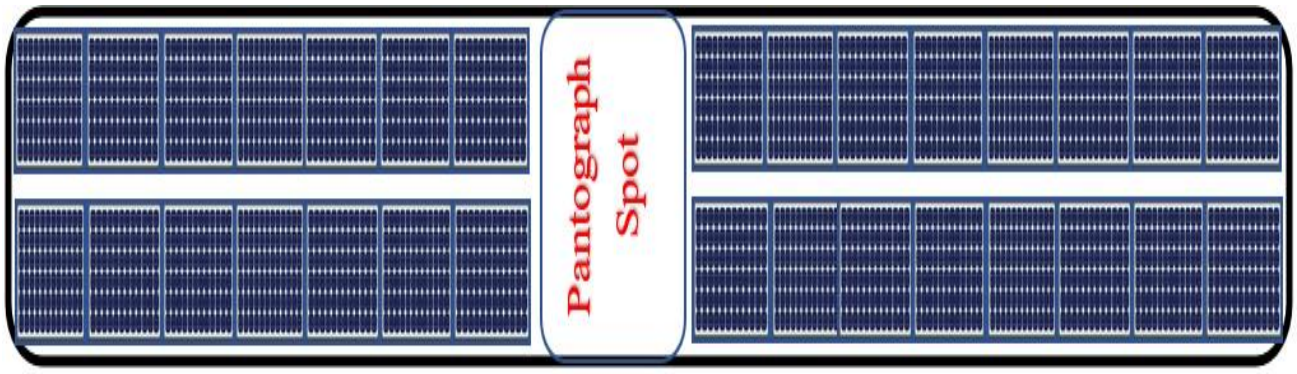

Figure 3. 2: Potential arrangement of the PV Modules on the Train Roof

MODULE DIMENSIONS (mm)

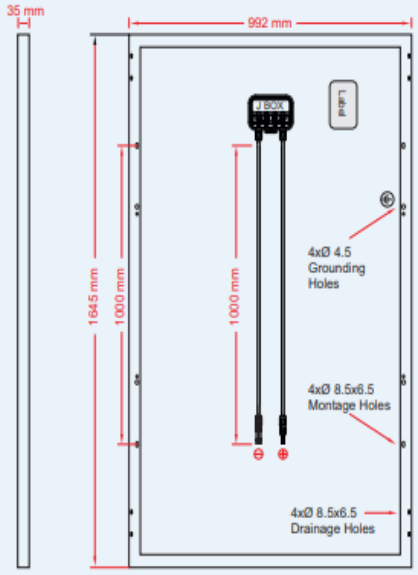

CURRENT VOLTAGE CURVE

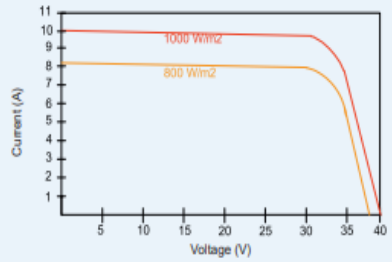

POWER VOLTAGE CURVE

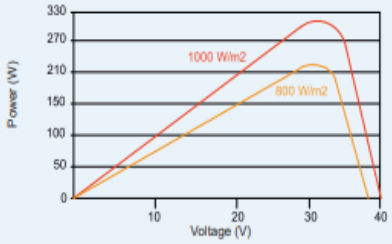

CURRENT VOLTAGE CURVE

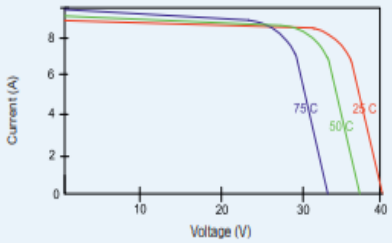

ELECTRICAL PARAMETERS (STC)

	Unit	OSM60-300W	OSM60-305W	OSMp60-310W	OSMp60-315W	OSMp60-320W
Maximum Power	Pmaks (Wp)	300	305	310	315	320
Positive Output Tolerance	0 ~ +5W					
Max. Power Voltage	Vmpp (V)	32,7	32,9	33,01	33,04	33,7
Max. Power Current	Impp (A)	9,2	9,28	9,41	9,5	9,55
Open Circuit Voltage	Voc (V)	39,8	40,3	40,6	40,7	40,9
Short Circuit Voltage	Isc (A)	9,77	9,79	9,922	10,01	10,3
Module Efficiency	η_m (%)	18,44	18,74	19,05	19,36	19,66

STC: 1000W/m² Irradiation / 25°C Cell Temperature / AM=1,5 / Measurement Accuracy ±%3 / 1m/s Wind Speed

ELECTRICAL PARAMETERS (NOTC)

	Unit	OSM60-300W	OSM60-305W	OSMp60-310W	OSMp60-315W	OSMp60-320W
Maximum Power	Pmaks (Wp)	223	225	232	235	239
Max. Power Voltage	Vmpp (V)	30,2	30,5	30,9	31,3	31,5
Max. Power Current	Impp (A)	7,39	7,45	7,5	7,57	7,58
Open Circuit Voltage	Voc (V)	37	37,3	37,5	37,6	37,9
Short Circuit Voltage	Isc (A)	7,89	7,9	8,21	8,33	8,45

NOTC: 800W/m² Irradiation / 20°C Cell Temperature / AM=1,5 / Measurement Accuracy ±%3 / 1m/s Wind Speed

MECHANICAL COMPONENTS

Cell Type	Monocrystalline Perc Cell / 156.75 mm x 156.75 mm
Cell Amount	60 Cell (6x10)
Panel Size	992 x 1645 x 35 mm
Weight	19 Kg
Glass	3.2 mm (0,125")Low Ironed High-Pass Tempered Glass
Back Surface	Multi Layered White Polimer Film
Frame	White Anodized Aluminium
Junction Box	IP 67 or IP 68 - 1500 VDC / 15A
Output Cables	IEC, UL approved (4 mm² ,12 AWG) (PV Cable Type) , 1000mm
Connector	Compatible MC4 (IP67, IEC and UL approved)
Fire Resistance	Type 1, Type 2 - A Class
Impact Resistance	Decreased from "51,19 / 1300 mm, (1.18 lbs / 535g) Steel Ball Test

TEMPERATURE COEFFICIENTS

NOTC (Nominal Cell Working Temperature)	45°C (± 2°C)
Temperaure Coefficent (Pmax)	-0,40 %/°C
Temperaure Coefficent (Voc)	-0,3409 %/°C
Temperaure Coefficent (Isc)	+0,0447 %/°C

WORKING CONDITIONS

Working Temperature	-40~+85°C
Max. System Voltage	1500V DC (UL / IEC)
Max. Reverse Current	15A / 20A
Maximum Load	75 lbs ft (UL Standard) 5400 Pa (IEC Standard)

Figure 3. 3: Datasheet for the 320W Monocrystalline Module OSMp60-320W

Table 3. 2: Number of PV Panels Calculation and Arrangement

Total roof Area	$29.4m \times 2.65m = \mathbf{77.91\ m^2}$
Effective Area	$27.4m \times 1.984m = \mathbf{54.36\ m^2}$
For 72 cells,	
One Solar Panel Area	$1.689m \times 0.992m = 1.675\ m^2$
No. of Solar Panels	$\frac{54.36}{1.675} = 32.5$
16 panels longitudinally	$16 \times 1.689m = \mathbf{24.75m < 29.4m}$
2panels transversally	$2 \times 0.99m = \mathbf{1.984m < 2.65m}$

It is very necessary to compute the total weight of the PV panels because placing panels on the roof of the rolling train alter the total weight, thus increasing the energy consumption.

The Weight of one PV panel is 19 kg and total mass is obtained by multiplying the mass of one panel by the number of available PV panels Thus,

$$Total\ Weight = 19kg \times 32 = 608kg = 0.608\ tonne.$$

This mass should also be considered while computing the real energy consumption by train since it can alter the traction power consumption.

The upper limit loading on rooftops is considered at 97.6 kg/m2 to maintain low risk of structural collapse, damage, or system failure. For this application, a factor of safety of 4 has also been considered to reduce the possible risk of structural damage due to unforeseen loads including wind, captured water, hail crystals from rain, or perhaps even living creatures like birds.

Depending on that, the total tolerable load upon on roof will be 97.6/4 = 24.4 kg/m^2.

Because a 1.65 m2 solar panel weighs approximately 19 kg, the load capacity of panels is 19 kg /1.65 m^2 = 11.5 which is less than the allowable load limit of 24.4 kg/m^2.

As a result, we have no issues with overburdening from modules.

3.1.2 Calculation of the PV Power and Energy Harnessed from the Panels Mounted on the Train Roof.

When it comes to Power calculation from solar array, there are always two scenarios: we can either start from the power demand or power that is needed and use it to select the suitable panels and compute the required area. Or we can start from a fixed area and compute the power and number of panels. In this work, the second scenario has been implemented since the area of the train roof is fixed. There are some determinant factors for computing the power from rooftop PV, these includes: Effective available area, type and efficiency of PV cells, solar radiation angle, sunshine, location and weather conditions.

The total power per day can be calculated by the expression (6) from reference [9], [44], [45]:

$$P_T = G \times A_e \times \eta_{sc} \times \eta_{MPPT} \times K_c \quad (6)$$

Where P_T is PV power generation per day; $G$is monthly average daily global radiation on a horizontal surface; A_e is effective area of the rooftop; η_{sc} is solar cell efficiency; η_{MPPT} is MPPT efficiency and K_c is clear sky index.

The following Angstrom-Prescott (A-P) relation (7) cited in [46] can be used to calculate the monthly average daily global solar radiation on a horizontal surface:

$$\frac{G}{G_0} = (a + b)\left(\frac{S}{S_M}\right) \quad (7)$$

Where G_0 is the monthly daily average extraterrestrial radiation on horizontal surface a, b are the Angstrom regression constants; S is the monthly average daily hours of bright sunshine; S_M is the monthly average daily number of hours of possible sunshine (day light between sunrise and sunset).

The most widely used parameter in sunshine-based models for estimating global solar radiation is sunshine period. Sunshine duration is described as the amount of all thread in which direct solar irradiance exceeds 120Wm-2 [47].

The solar declination (δ) and mean sunrise hour angle (ω_s) for a typical day could be calculated using equations (8) and (9) as shown in [47]:

$$\delta = 23.45^0 \times \sin\left(360\frac{284+n}{365}\right) = -17.78^0 \quad (8)$$

$$\omega_s = cos^{-1}(\tan\Phi \tan\delta) = 92.9^0 \quad (9)$$

Where n is the number of days starting from January 1st ($n = 31$) and Φ is the latitude of the considered region (Addis Ababa = 8.98^0) and δ is the solar declination.

Now, G_0 can be calculated in (10) as in [46]:

$$G_0 = \left(\frac{24}{\pi}\right) GSC \left[1 + 0.033cos\left(\frac{360n}{365}\right)\right] \times \left[\cos\Phi \cos\delta \sin\omega_s + \frac{\pi\omega_s}{180}\sin\Phi \sin\delta\right] \quad (10)$$

Where GSC is the solar constant and it is equal to 1367W/m^2

The monthly average daily number of hours of possible sunshine S_M in equation (7) is determined from equation (11) as in [46]–[48]:

$$S_M = \frac{2}{15} cos^{-1}(\tan\Phi \tan\delta) \quad (11)$$

The Angstrom regression coefficient **a** and **b** are calculated from the following expressions as in [47]:

$$a = 0.1 + 0.24\left(\frac{S}{S_M}\right) \quad (12)$$

$$b = 0.38 + 0.08\left(\frac{S}{S_M}\right) \quad (13)$$

The monthly average daily hours of bright sunshine S is calculated in equation (14) as in [46], [48]:

$$S = S_s - S_r \quad (14)$$

Where S_s is sunset and S_r is sunrise

$$S_r = 12 - \frac{1}{15^0} cos^{-1}\left(\frac{-\sin\Phi \sin\delta}{\cos\Phi \cos\delta}\right) \quad (15)$$

$$S_s = 12 + \frac{1}{15^0} cos^{-1}\left(\frac{-\sin\Phi \sin\delta}{\cos\Phi \cos\delta}\right) \quad (16)$$

Table 3. 3: Summarized Yearly Distribution of Radiation in Addis Ababa.

Month	n in days	Φin (^{0})	δin (^{0})	$\omega_s$in (^{0})	Sin (hrs)	$S_M$in (hrs)	G_0in kWh/m^2/d	G in kWh/m^2/d
Jan.	31	8.98	-17.78	92.9	11.6	12.38	9.258	6.77
Feb.	59	8.98	-8.67	91.3	11.7	12.17	9.973	7.56
Mar.	90	8.98	3.61	89.42	11.8	11.92	10.46	7.26
Apr.	120	8.98	14.58	87.64	11.9	11.68	10.44	6.58
May	151	8.98	21.89	86.35	12	11.51	10.17	6.62
June	181	8.98	23.18	86.12	12	11.48	10.08	5.56
July	212	8.98	18.17	87.02	12	11.60	10.26	6.61
Aug.	243	8.98	8.10	88.71	11.8	11.82	10.39	6.30
Sept.	273	8.98	-3.81	90.6	11.7	12.08	10.12	7.73
Oct.	304	8.98	-15.05	92.43	11.6	12.32	9.422	6.93
Nov.	334	8.98	-21.96	93.65	11.5	12.48	8.794	6.28
Dec.	365	8.98	-23.08	93.86	11.5	12.51	8.699	6.20
Mean								**6.70**

Therefore, the average horizontal radiation value in Addis Ababa and its surrounding is around 6.7kWh/m^2/day, in other words: in an average day (approximatlety13 hours from sunrise to sunset) the total energy radiated by the sun onto 1 square meter is 6.7kWh. We would obtain the same amount of energy if radiation exposure were compressed, so to say 6.7 hours and the STC standard radiation of 1kW/m^2 was radiated onto a surface of 1 square meter. With this in mind, it is now possible to provide an interpretation of the measure of the module output Watt-peak (Wp). As mentioned in the previous section, let us consider a 320 Wp module that lies flat on the roof of the moving train as a key of our study. The module would supply its peak output, also referred to as nominal output of 320 Watts for 6.7hours. This result in a daily energy yield as expressed in equation (17):

$$E_{PV} = P_{PV} \times t \times n \qquad (17)$$

Where E_{PV} is the PV energy; P_{PV} is the PV power; t is the unit time; n is the number of panels.

3.1.3 Onboard Auxiliary Energy Modeling and Optimization

Door opening control motors, displays, magnetic braking system, Lighting, air conditioning, and other auxiliary equipment are examples of auxiliary equipment. In the simulation, assume that all auxiliary equipment is always operational (worst case scenario). The power usage can then be computed using the following equation (18) as in [49]:

$$E_a = \frac{P_a \times t_a}{3600} = \frac{(P_{am} \times n_m + P_{at} \times n_t) \times t_a}{3600} \quad (18)$$

Where: E_a is total energy consumption of auxiliary equipment in (kWh); P_a is total electric power for auxiliary equipment in (kW); t_a is train operation time in (sec); P_{am} is electric power per locomotive car in (kW); n_m is number of locomotive cars; P_{at} is electric power per trailer car; and n_t is number of trailer car.

From the data reported in table 3.4, we realize that there are three main components that constitute the auxiliary power supply box to consider in this design. These are the battery sets, the auxiliary inverter, and the air conditioning unit.

Table 3. 4: AALRT Auxiliary Power Supply Components Specifications

Component	Description	Technical parameters
Auxiliary Power Supply (APS)	• APS Box obtains DC 750V from the contact network. • APS includes auxiliary inverter and batteries. • All across the train, there are two APS systems.	• Designed capacity: 35kVA. • Voltage at Input: DC 750V • APS Voltage range: DC 500V--900V • Voltage at Output: 3-phase 380V, single-phase 220V • Output Frequency: 50Hz ± 1% • Overall dimension: 1,782mm(L)×900mm(W)×495mm(H);
Auxiliary inverter	• Consists of IGBT inverter power unit, 3-phase isolation transformer, logic control unit and filter capacitor.	• Max. output power: 8kW • Input voltage range: 500V～1000V • Rater input current: DC53A • Control system voltage: DC24V • Conversion efficiency: ≥80% • Output voltage: AC 380V

	• It works by converting 750 VDC into 3-phase 380VAC	
Charger		• Rated output power: 8kW • Output voltage range: DC24V~29V • Temperature compensation factor: -4mV/℃ • Battery charging current limit: 25A • Output ripple voltage: ≤1.5V • Max. output current: DC330A • Conversion efficiency: ≥80% • Ambient Temperature: 0℃~29.7℃
Battery	• There are 2 battery sets. • Each battery set has 19 pieces. • The battery pieces are connected in series for capacity and efficiency optimization.	• Battery type: Ni-Cd battery • Total nominal voltage: 24 V • Operating voltage: 24-29VDC • Operating environmental Temperature: -40℃~60℃ • Capacity: 100Ah • Float charging voltage: 1.45~1.55V/cell • Rated voltage: 1.2V/cell
Air Conditioning unity (AC)	• It has a fresh air outlet with a water-retaining louver. • In the winter, a device for preheating and filtering fresh air is installed. • Two sets of air conditioning units for each train	• Input power = 12.7kw • Cooling capacity = 25kw • Air supply rate = 4000m^3/h • Refrigerant charge = 2×2.4 kg • Weight = 600kg • Main loop three phase 380VAC / 50Hz • Control loop = DC24V

According to the power ratings of these components, it is observed that the power harvested from 32 PV panels, reported in the previous section, is not enough to cater all the onboard auxiliary loads. It is therefore critical to assess possible strategies to optimize the configuration of this

system. Therefore, for the optimization purpose, the air conditioning unit has been left out in this configuration, for its power requirement is beyond the capability of our PV array output power.

It is however worth noting that in the case of AALRT, the air conditioning unit is not used at its full capacity. The device was designed to suit the standards but was not customized to the requirements of a country like Ethiopia. The seasonal changes are not significant, and the temperature is relatively conducive. In the case of AALRT, only the cooling system is utilized to keep the passenger saloon cooled and ventilated. This translates to the air conditioning unit being underutilized, and consequently inefficiently used.

The data collected show the power ratings of the onboard auxiliary power supply components. The auxiliary inverter with a maximum rated output power of 8kW takes catenary voltage in the range of 500V～1000V and supplies the AC loads. The battery charger is rated at a maximum power of 8kW as well and charges the batteries with an operating voltage of 24-29VDC. The batteries are able to keep all auxiliary dc loads functioning, so it can be concluded that a total power of 8kW is needed to keep all DC loads operating. The air conditioning unit is rated at 12.7kW and this power requirement is beyond the capacity of the PV and the battery system. Considering the worst-case scenario, the total operation time is 16 hours (from 6:00 AM to 10:00 PM), and the total energy requirement for the onboard auxiliary DC loads can be calculated using equation (18).

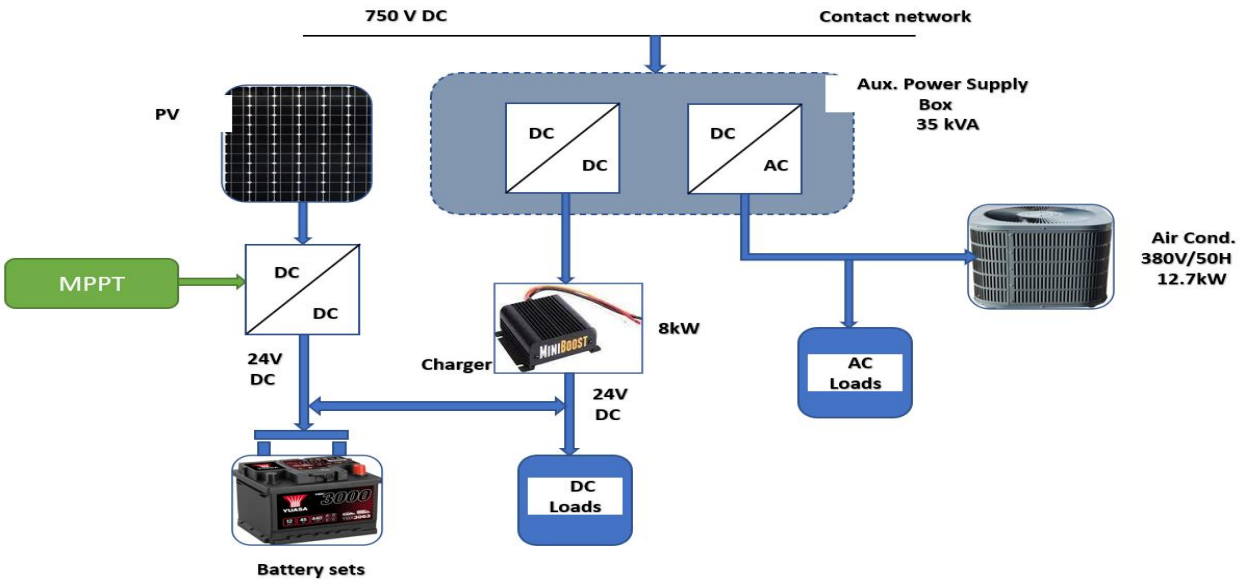

Figure 3. 4: Synoptic Diagram of the System Configuration

Considering STC, it has been demonstrated that in Addis Ababa and its surrounding, we can have 6.7 hours of sunshine per day. Accordingly, the total energy harvested can be calculated in equation (17).

The battery set capacity has been given as 100Ah with maximum charge current of 25A. this information can help us to determine the battery charging time and how much energy it can deliver when fully charged. It is worth mentioning that the train battery system is composed of two (2) battery sets with nineteen (19) pieces of Nickel Cadmium Alkaline battery each as shown in figure 3.5. For capacity optimization and efficiency, the battery pieces are connected in series to raise their individual nominal voltage of 1.2 V to a total operation voltage of around 24V.

Figure 3. 5: One Installed Battery Set of 19 Individual Batteries.

Battery different parameters can be calculated using equations reported in [50], [51]

Battery charging time given by:

$$Tc = \frac{C_b}{Ic} \tag{19}$$

Battery energy is given by:

$$E_b = \frac{C_b \times k \times V_b}{A_b} \tag{20}$$

Where T_c is the battery charging time in (hrs.); I_c is the charging current in (A); C_b is battery capacity in Ah; E_b is Total battery energy per day (kWh/d); V_b is the battery nominal voltage; A_b battery autonomy in days; k is the depth of discharge coefficient.

When fully charged, the battery run time or battery autonomy can also be computed using the formula:

$$A_b = \frac{n \times C_b \times k \times V_b}{E_b} \tag{21}$$

Where E_a is total energy consumption of auxiliary equipment in (kWh), n is the number of battery sets.

Figure 3. 6: Ni_Cd Alkaline Battery Set at AALRT (in maintenance room)

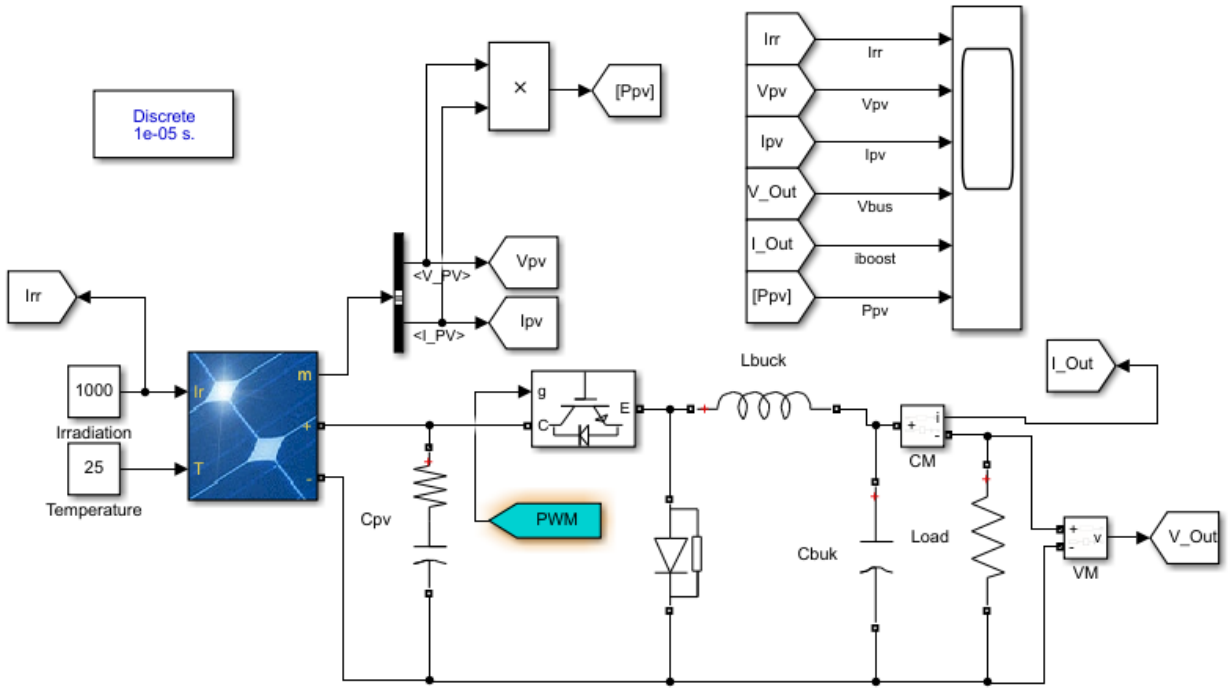

Figure 3. 7:PV Array Simulink with Buck Converter

The solar photovoltaic array above has been designed according to the specifications and calculations determined in the previous section. Given the fixed available area on the rooftop of the train, a total number of 32 modules can be installed. The potential distribution on the available area is shown in the figure 3.2. The array is connected to a simple buck DC-DC converter, which scales down the large input voltage level from the solar array into such a minimal output voltage for the battery sets and for dc loads as depicted in figure 3.7. The input of the buck converter is connected to the PV array through an RC branch to achieve the MPP in various meteorological conditions. The dc input capacitor denoted C_{pv} is used to avoid significant PV voltage fluctuations while the resistor controls the input current. The purely resistive load at the output side of the buck converter is represents a dc load and is considered as a dc bus in the simulation. A back-stepping configuration is used in the DC-DC converter to monitor the photovoltaic reference voltage produced by the MPPT component, as described in the preceding section. Using a PWM generator, this controller helps to create a appropriate duty cycle for regulating a power transistor of the buck converter. The inductance L and capacitance C are given by the expressions in equation (22) and equation (23) respectively [52].

$$\text{Inductance, } L = \frac{V_{op}(V_{ip}-V_{op})}{f_{sw}\times\Delta I\times V_{ip}} \tag{22}$$

$$\text{Capacitance, } C = \frac{\Delta I}{f_{sw}\times\Delta V\times 8} \tag{23}$$

Where $V_{ip}$is the input voltage; V_{op} is the output voltage; f_{sw} is the switching frequency; ΔI is the current ripple of the input current; ΔV is the voltage ripple of the output voltage.

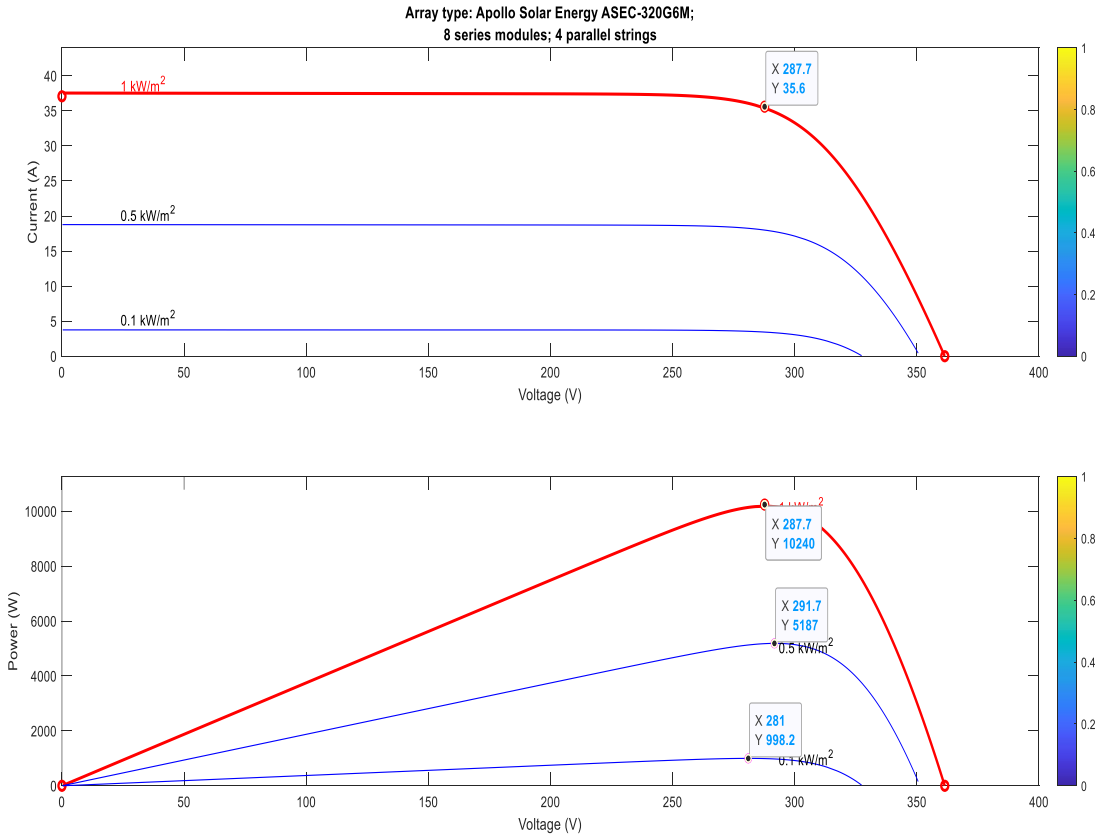

Figure 3. 8: I-V and P-V Characteristics

3.2 The Maximum Power Point Tracking

The perturb and observe tracking technique is adopted to track the solar array voltage in this work, which leads to an increase or decrease in power, as can be seen in figure 3.8. If a voltage increase causes a power to increase, this indicates that the operating point is to the left of the MPP and that further voltage perturbation to the right is required to reach the MPP. If, on the other hand, a rise

in voltage causes a drop in power, this suggest that the actual operating point would be to the right of the MPP and that additional voltage disturbance to the left is needed to reinstate the MPP.

As a result of these perturbations, the algorithm eventually converges on the MPP. The P&O algorithm makes use of the fact that the P-V curve decreases to the right of the MPP and increases to the left of the MPP. The disadvantage of this method/technique is that the MPP's operating point is almost never stabilized and consistent. It's always fluctuating in the MPP vicinity. This can be minimized by making small perturbation steps near the MPP (or a PI controller).

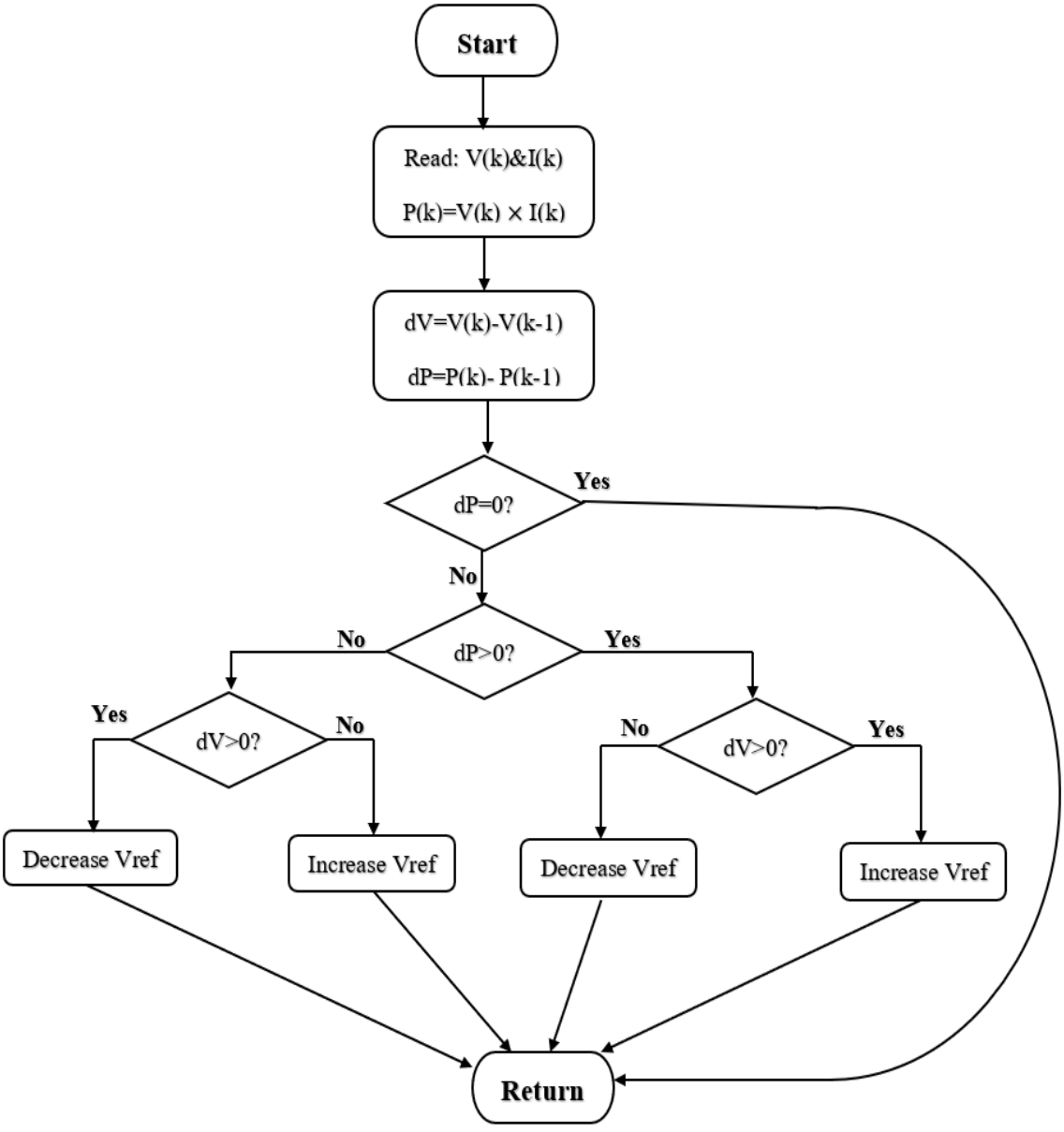

Figure 3. 9: MPPT Algorithm Flowchart

There are basically two ways we can implement MPPT in a buck converter: First, we send both PV voltage (Vpv) and current (Ipv) and with the help of these values, we implement the MPPT. The MPPT output instantly provides the needed duty ratio for PWM generation, this value is then compared to the carrier signal and fed into the IGBT.

With the second approach, which is similar to the first, we give the voltage and current before implementing the MPPT. However, rather than a duty ratio, we obtain a reference voltage at the output in this case. This reference voltage is contrasted to the real PV voltage to determine the error; the error is then supplied to a PI controller, whose output gives the duty ratio needed for PWM generation; this value is then compared to the carrier signal and fed to the IGBT.

This method outperforms the first in terms of MPPT tracking performance because it uses a closed loop control mechanism. This method was used in this project.

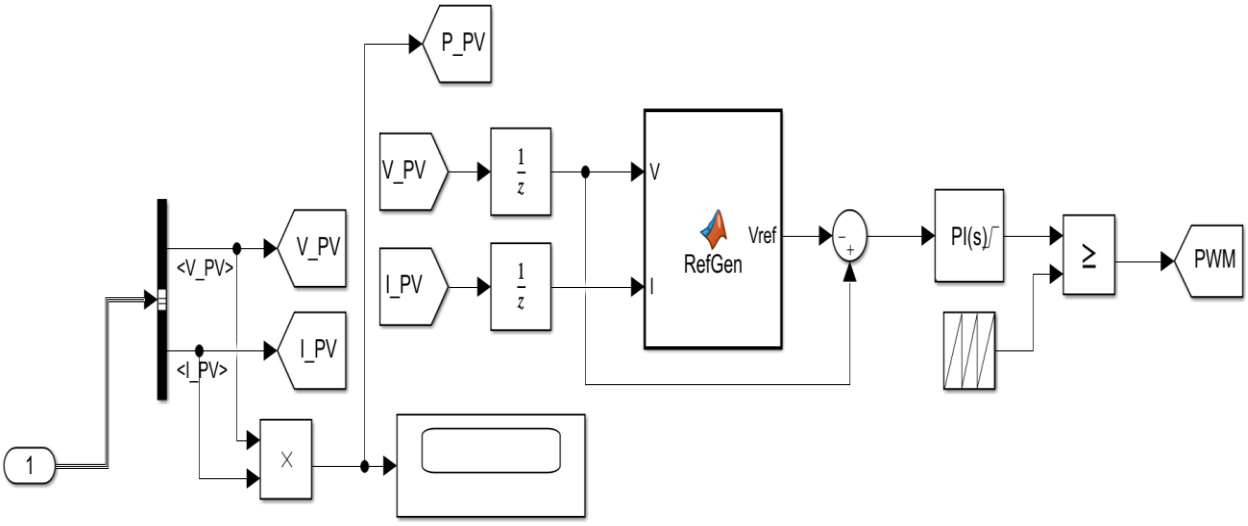

Figure 3. 10: MPPT Simulink Model

The block diagram shown in figure 3.10 above represent the Simulink model of the MPPT tracking algorithm. The MATLAB function denoted RefGen encloses the MPPT code from the algorithm described in the perturb and observe MPPT flowchart described in figure 3.9. The unit delay blocks have been added in order to avoid errors sometimes shown by MATLAB in evaluating the PV array values. The PI Controller is added and its K_P and K_I and values are set accordingly to control the variations in the power curve.

3.3 Control Strategy of the Battery Management System

The battery management system is designed here to be able to control the energy flow within the system. The algorithm is shown in the flowchart of figure 3.11 below. The functional principles of this control scheme of the battery pack system gives priority to the onboard auxiliary loads.

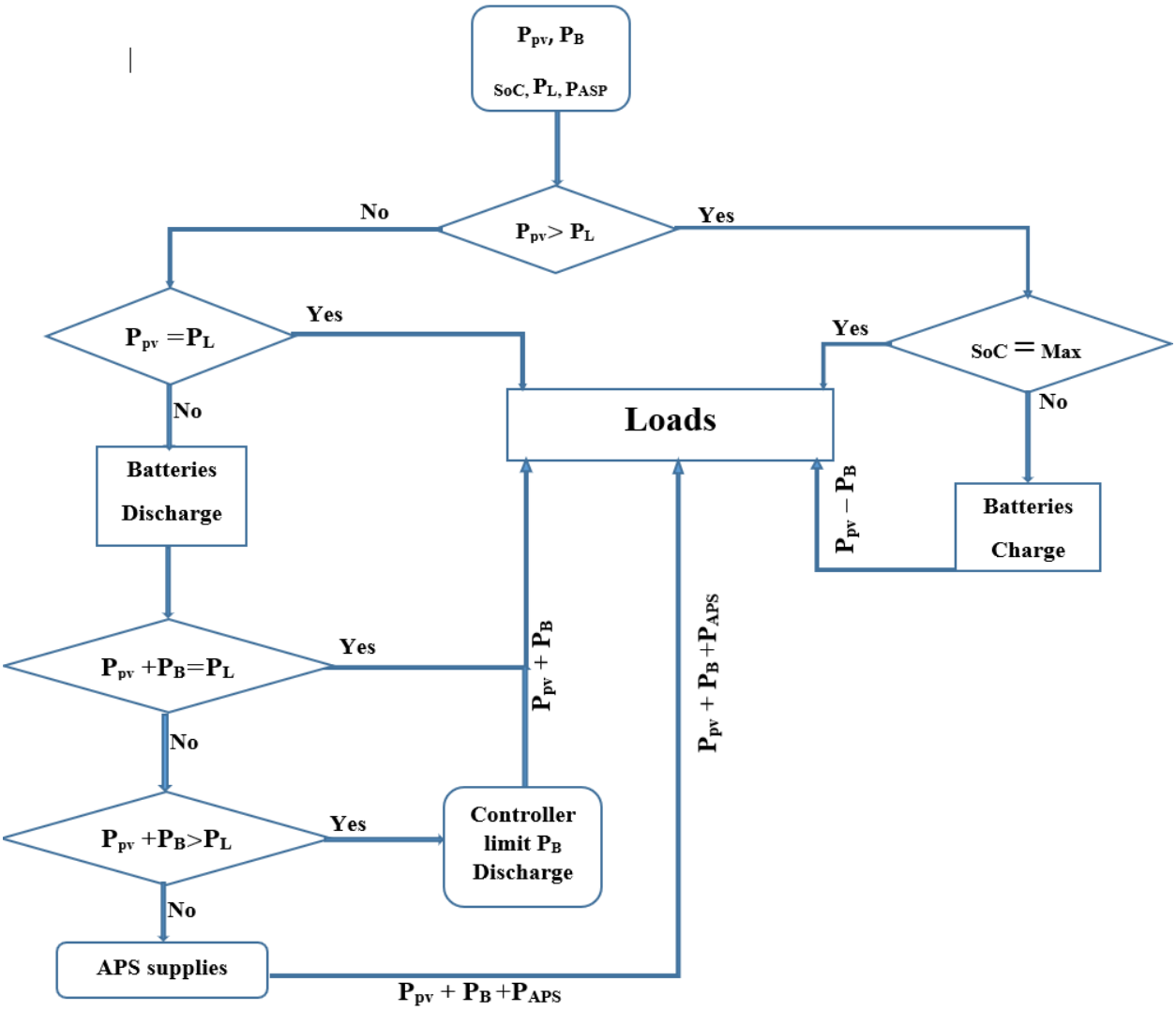

Figure 3. 11: Battery Management System Flowchart

It considers solar array output power $\mathbf{P_{pv}}$, the battery energy storage power $\mathbf{P_{battery}}$, the battery state of charge **SOC**, the total auxiliary $\mathbf{P_{load}}$ and the auxiliary power supply power $\mathbf{P_{APS}}$, then perform the following:

1) When $\mathbf{P_{pv} > P_{load}}$, the solar array output power or PV power will be prioritized feeding the onboard auxiliary loads of the trains. Then the remaining power from the PV is used for to

charge the battery sets up to maximum SOC of 100 percent, where the power to the battery is $\mathbf{P_{pv} - P_{load}}$.

2) When $\mathbf{P_{pv} = P_{load}}$, Only the output power from the solar PV array supply train's onboard auxiliary loads are powered, and the battery is idle.

3) When $\mathbf{P_{pv} < P_{load}}$, the solar system output power supplies the train's auxiliary, but also the battery discharges its power, so SOC values must be greater than 10%. Therefore, the total power to satisfy the load requirement is equal to $\mathbf{P_{pv} + P_{battery}}$. At this point:

   a) When $\mathbf{P_{pv} + P_{battery} > P_{load}}$, control strategy algorithm regulates the charging power of the battery sets.

   b) When $\mathbf{P_{pv} + P_{battery} < P_{load}}$, the extra power to cater for the demand will be drawn from the normal auxiliary power supply system and the total will be equal to the sum of all the three power sources as $\mathbf{P_{pv} + P_{battery} + P_{APS}}$.

As per the above described control scheme, the BMS must send different instructions in various working conditions in order to control the system's devices. Finally, by using this control strategy, BMS can perform the energy management function.

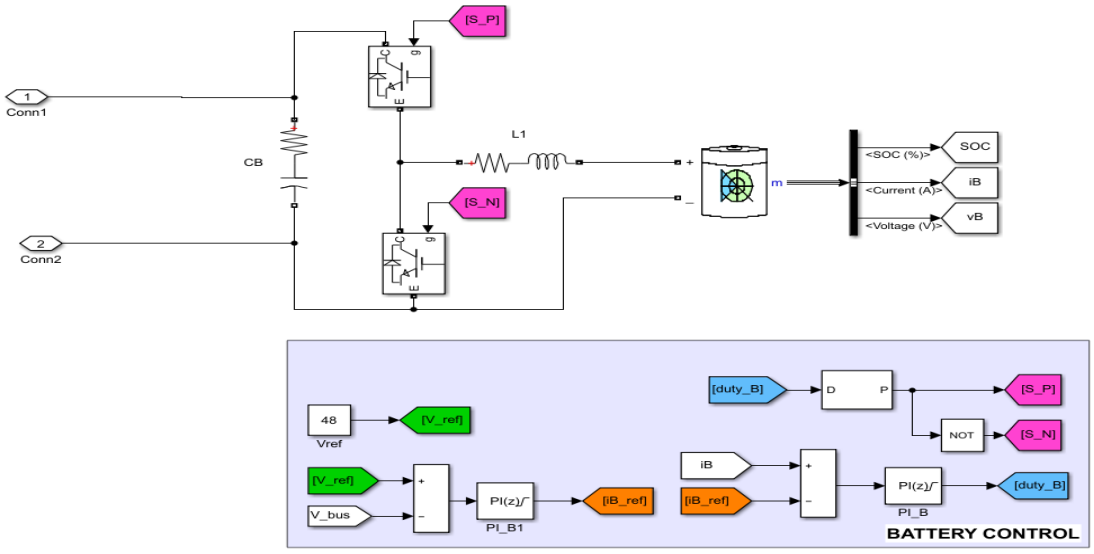

Figure 3. 12: Simulink Model of the Battery Component and its Control

A bidirectional DC-DC converter connects the battery to the dc bus since it works both in charging and discharging mode as described in the flowchart of figure 2.11. The battery side capacitor (RC) is added to limit the current and control voltage fluctuation at the battery charging ports.in this design the battery management system is implemented in two stages working together, namely

constant current control and constant voltage control. The PI controller is needed to generate the duty signal. In this design, two PI controllers are used, one for determining the battery reference current (the current control PI) and the other one for determining the battery voltage reference (the voltage control PI). For the case of constant current control, the error between the battery current and the reference current is added to the input of current control PI to control the battery current. The same is applied for the case of constant voltage control.

The dc-dc PWM signal generator is used to generate the signals, duty signal is fed to the input of the PWM generator.

3.4 Economic Evaluation of the Proposed System

There are a variety of direct approaches for determining the profitability of a project. The economic factors evaluated in this study are intended to assess the effectiveness of placing a PV array on the train roof for the proposed system. Payback Period is one of the methods for determining a project's economic value, and it is defined as in equation (24) according to[53] .

On the basis of current market prices, the PV panels' investment cost and running cost can be calculated. Due to mass production, the price of PV modules is currently decreasing in relation to the application area.

$$PB_p = \frac{C_{out}}{C_{in}} \tag{24}$$

Where PB_p is the payback period; C_{out} is Cash-out which represent the initial investment cost; C_{in} is Cash-in which represent the Cash inflow per year.

With this parameter, the higher the payback period, the less profitable the project is in terms of cash inflow. The technology is expected to have a longer payback period in this study because the primary purpose is to lessen reliance on the national grid rather than make money.

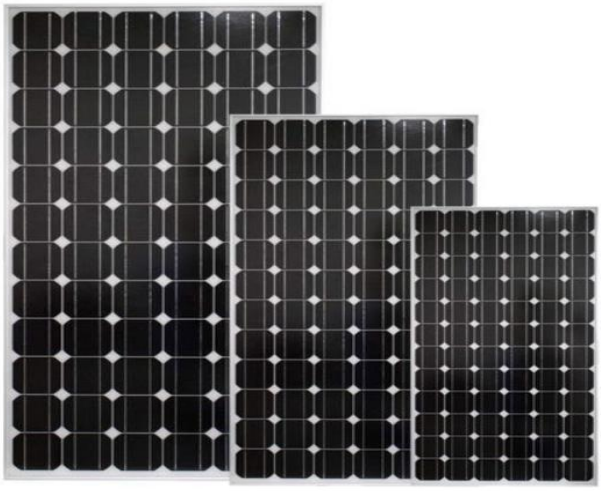

Figure 3. 13:Monocrystalline Solar Panel OSMp60-320W

The temporal worth of money is not taken into account by this parameter, which is one of its flaws. It is worth noting that today's money is worth a lot more than money that will be created in the future. Figure 3.12 and figure 3.13 show the solar panel and the MPPT converter models that have been considered in this research, respectively. The market prices considered in this study for the particular devices have been taken from amazon and the reflect the actual value at the market. The PV panels are evaluated at the price of $0.22/Wp whereas the MPPT is evaluated at $700.

Figure 3. 14: Solar MPPT Battery Charger Controller (XD-384V)

In the previous sections, it has been demonstrated that PV array and batteries alone cannot supply the whole auxiliary power supply system. The air conditioning unit has been left out in this design due to its huge amount of power requirement. Some AC loads such us passenger saloon lights have not been considered in this design to avoid unnecessary extra cost of an inverter. However, this research briefly explores the possibility of taking advantage of the regenerative braking energy to supply the other auxiliary AC loads. The modeling of this regenerative braking is detailed in the next section.

3.5 Regenerative Braking Energy Modelling

Today's advanced electric train systems are fitted out with regenerative braking systems in which some energy is generated from the train's kinetics during the braking. Note that the train's braking force is composed of friction braking force and motor braking force which is the force the motor uses to generate electricity. Thus, equation (25) must be applied to determine the electric braking force first [49], then the product of the motor braking force, velocity and regenerative efficiency yield the electric power produced by the regenerative braking in equation (26). It can be expressed as in [54], [55] as follow:

$$F_T = F_b + F_f \tag{25}$$

$$P_{reg} = \frac{1}{3.6} F_b \times V \times \eta_{reg}, \tag{26}$$

where F_T is the total braking force (kN), F_b is the regenerative braking force (kN), F_f is the friction braking force (kN), P_{reg} is the electric power regenerated from braking (kW), V is the speed of the train (m/s), η_{reg} is the efficiency of the regeneration system.

The power consumed during braking and regenerated power can be estimated based on the traction braking force which acts to decelerate and stop the train and has been expressed in [55] as:

$$M_{tot}\beta = -\left(F_b + F_g + F_r\right)$$

$$-F_b = M_{tot}\beta + F_g + F_r, \tag{27}$$

where M_{tot} is the total mass; F_b is the braking force (N); F_g is the force required to overcome the gravity; F_r is the force required to overcome train resistance and β is decerelation (m/s^2)

The power consumed to stop the motion is equal to the product of braking force F_B, and the change in velocity gives the power to be provided for braking:

$$P_{cons} = F_b + \Delta V, \tag{28}$$

Where P_{cons} is the power consumed during braking and ΔV is the change of speed during braking to stop.

It is possible to calculate the regenerated power for a break at stations as in equation (29):

$$P_{reg} = P_{cons} \times \eta_{reg},$$

$$\eta_{reg} = {1}\Big/{(e^{\frac{\alpha}{|a|}})}, \tag{29}$$

where **α** is the Optimum model parameter generally used as 0.65 for Asynchronous motor-driven machines), **a** is the maximum deceleration of the vehicle.

Integrating the power over the braking time yields the regenerated energy [54]:

$$E_{reg} = \int P_{reg} dt. \tag{30}$$

From this regenerative braking energy model, it is clear that its magnitude depends on a combination of many factors including efficiency of regeneration, braking time, deceleration, train mass, maximum operational speed, and all resistive forces.

3.7 Integration of the PV and Shading Analysis

The combined PV and battery energy storage system is incorporated on the roof of the vehicle. The Simulink block diagram of the system configuration is shown in figure 3.14. Maximum power point tracking control scheme is used for PV module integration and regulation to control the output power of the PV system in order to harvest maximum power from the PV. The famous perturb and observe algorithm is used to achieve MPPT control.

Hypothetically, voltage may increase/decrease beyond/below the allowable limit. To tackle this issue, battery sets are charged through the dc/dc charge controller to ensure the safe operation as shown in the figure 3.13 below. For the battery, the charging operation at the battery pack is

performed through constant current buck control and constant voltage buck control. The charge controller is included to save the batteries from overcharging and over discharging. It converts DC-DC power using Pulse Width Modulation signals of the electrical energy generated by the solar photovoltaic modules so as to convert it into an appropriate form. In practice, once the battery is fully charged, the PWM control will be applied to reduce the voltage level fed to the battery sets.

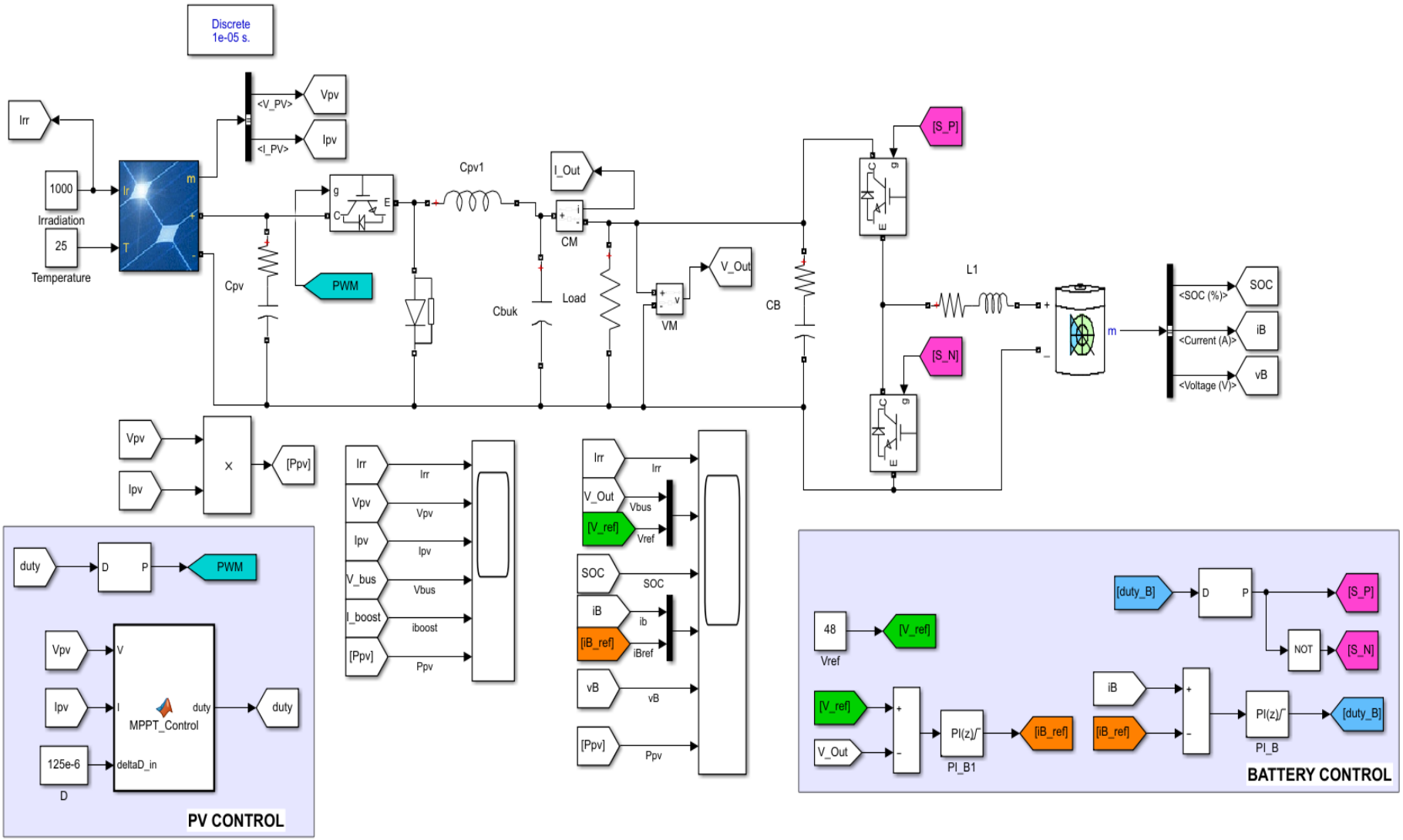

Figure 3. 15: Simulink Model of the Proposed System

3.8 Shading Analysis of the PV System

In the design phase for PV systems, shading scenarios create a unique problem. Objects in the immediate vicinity, such as buildings, can shade the PV generator partially or completely. The yield reduction is often more than one may expect based on the shadowed surface. As a result, shading analysis is an important part of PV system simulations.

Shading analysis is performed to capture the effect of shades on the moving panels mounted on roof of the railcar. This is achieved using PVsyst software based on the metrological data that are imported from the program database. The sun path is considered in these simulations to determine the tilt and azimuth angles in solar insolation striking the modules.

In this study, google earth is used to track the rail track surrounding for possible obstructions of sun irradiation. Two locations with a potential high shading impact were extracted as see in figures 3.15 and 3.16, and the shadow outline of these locations is recorded for the center point of the PV array.

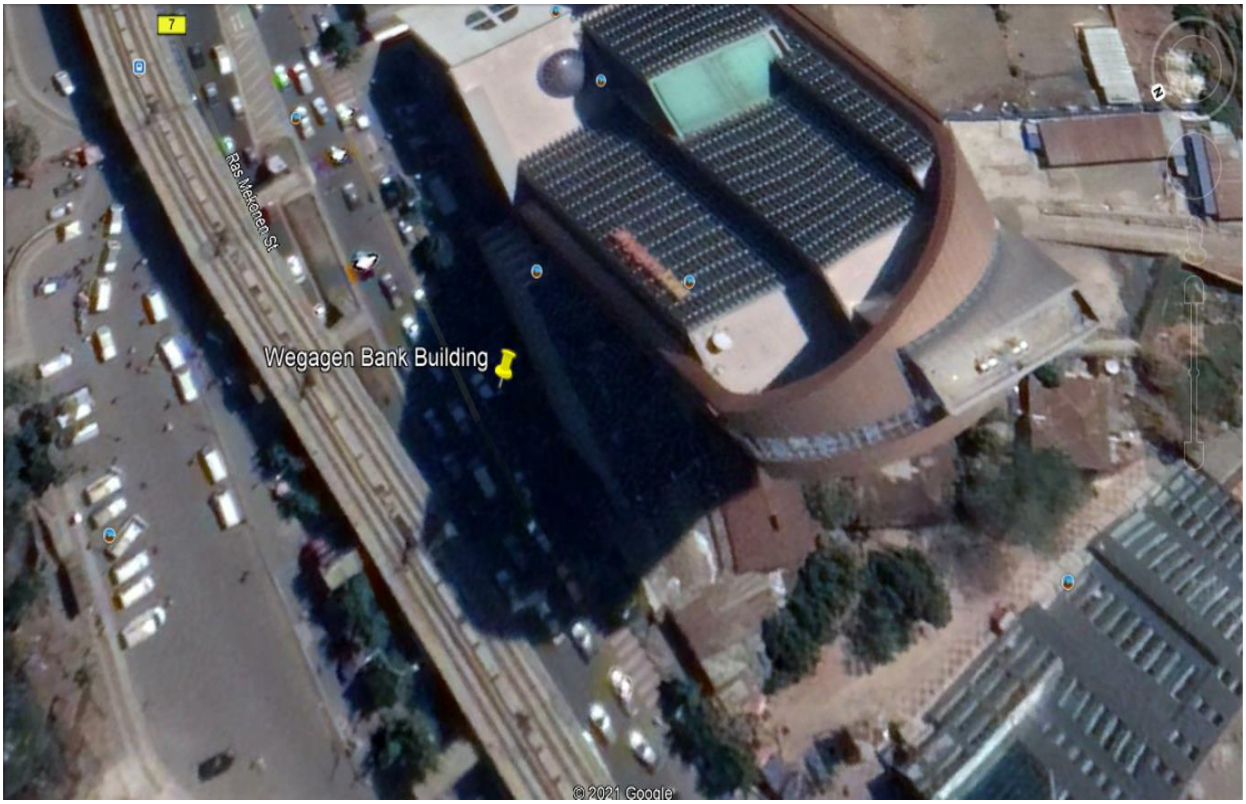

Figure 3. 16: Wegagen Bank Shadow Projection on the Track (near stadium)

Figure 3. 17: Capital Hotel Shadow Projection on the Track (hayahulet)

This is achieved using the site plan and sun path diagram. for this purpose, the distance and dimensions of the shadow-casting buildings are calculated. this information also helps us to calculate the azimuth angle and elevation angle.

The elevation angle is worked out for many obstacles in the vicinity of the rail track. The azimuth angle of the shadow-cast building is calculated using the equation (31):

$$Tan\,\gamma = \frac{h_2 - h_1}{d}$$

$$\gamma = arctan\left(\frac{h_2 - h_1}{d}\right) = \left(\frac{\Delta h}{d}\right) \qquad (31)$$

where γ is the azimuth angle, h_2 is the height of the building; h_1 is the height of surface from which the solar panels lie, Δh is the height difference and d is the distance from the building to the track.

The impact of shading on PV systems is determined by a variety of elements, including the percentage of shaded modules, the interconnection of cells and bypasses, the level of shading, the distribution pattern and shading over time, and the interconnection of panels, and so on.

PVSyst considers the shading effect's surface area in respect to predetermined strings or the full PV generator. This enables for a greater emphasis on shading effects from the string-by-string simulation, while bypass effects are ignored.

CHAPTER 4: RESULTS AND DISCUSSION

This chapter presents a detailed analysis and discussion of the results of the study pertaining to the objectives and methodologies described in previous chapters. The study proposed a photovoltaic power supply system to supply onboard auxiliary loads of the AALRT vehicles. For this to be achieved, various design and simulations were performed, and the results are presented. Power generation and Maximum Power Point Tracking performance are presented in the first part of this chapter. Subsequent sections present the Energy computation and analysis, the economic impact, and the shading situation of the proposed system. Regenerative braking energy has also been modelled for AC auxiliary loads that require high energy such as air conditioning unit.

4.1 Power Generation and Maximum Power Point Tracking Performance

The PV power generation is governed by the solar irradiation in a particular location of study and the maximum power point tracking system plays a defining role. In the case of Addis Ababa and its surrounding, a detailed study of the radiation distribution is performed, and the results are summarized in the figure 4.1. The resulting power is presented in figures 4.2 and 4.3 while the MPPT performance is portrayed in subsequent figures.

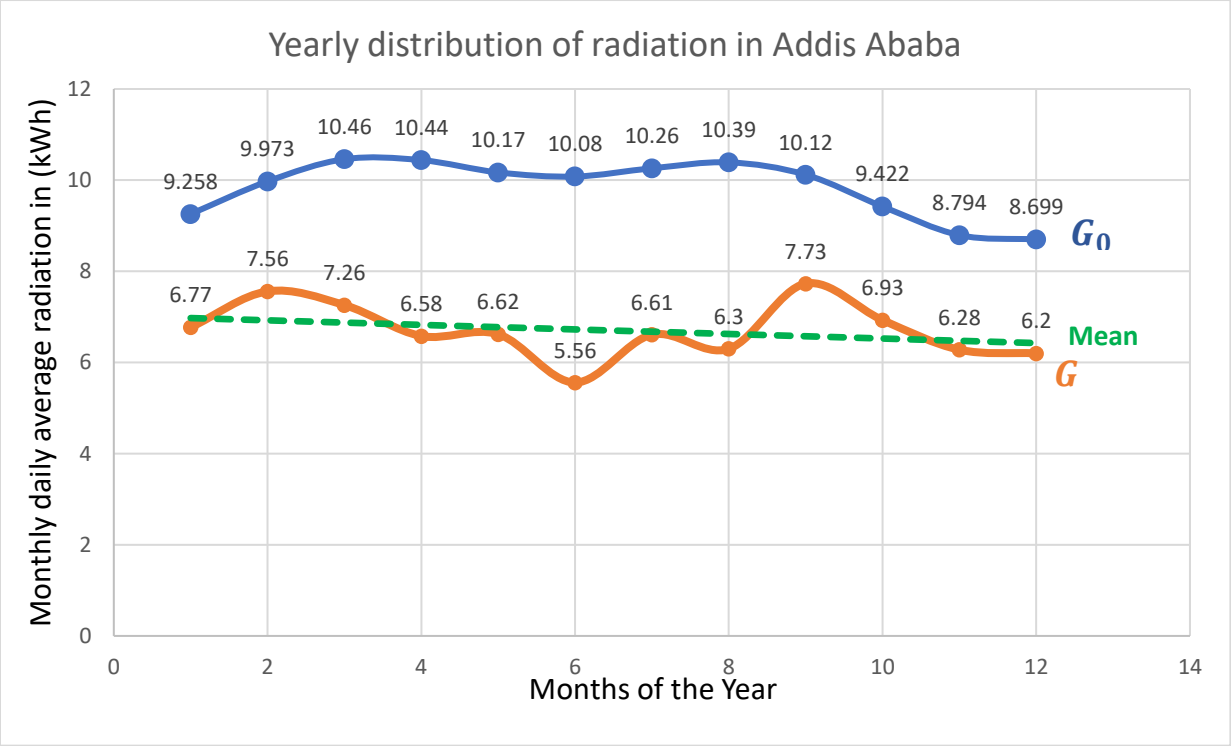

Figure 4. 1: Yearly Distribution of Irradiation in Addis Ababa

The figure 4.1 illustrates the summary of yearly distribution of radiation in Addis Ababa and its surrounding. From this graphical representation, the curves of main interest are the monthly average daily global radiation on a horizontal surface **G** in orange and the mean in green. These parameters play a defining role in the computation of the total PV output power of the proposed system. The mean value has been calculated and found to be 6.7kWh/m^2/day. This simply indicates that the total energy radiated by the sun onto 1 square meter in an ordinary day (about 13 hours from sunrise to sunset) is 6.7kWh.

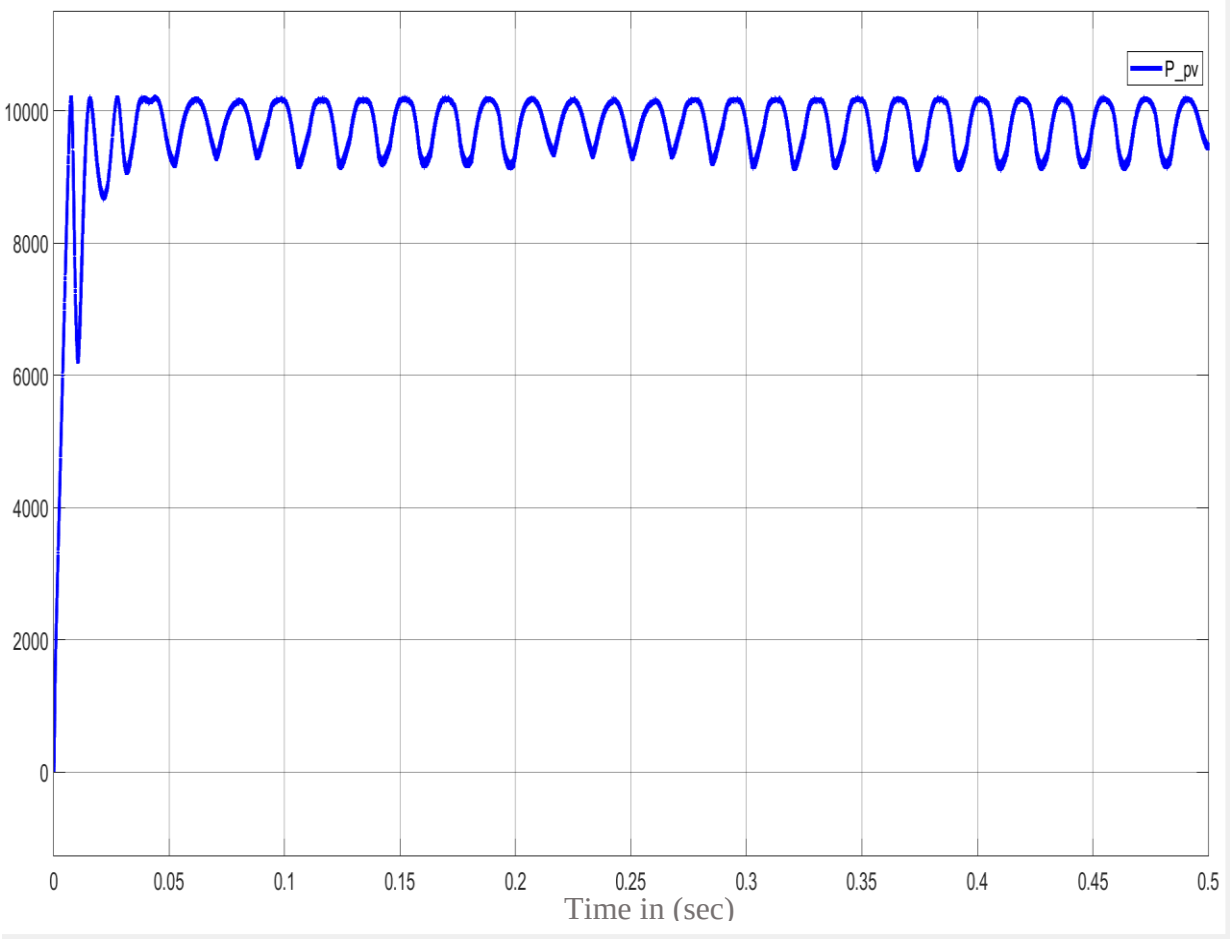

Figure 4. 2: PV Output Power without PI Controller

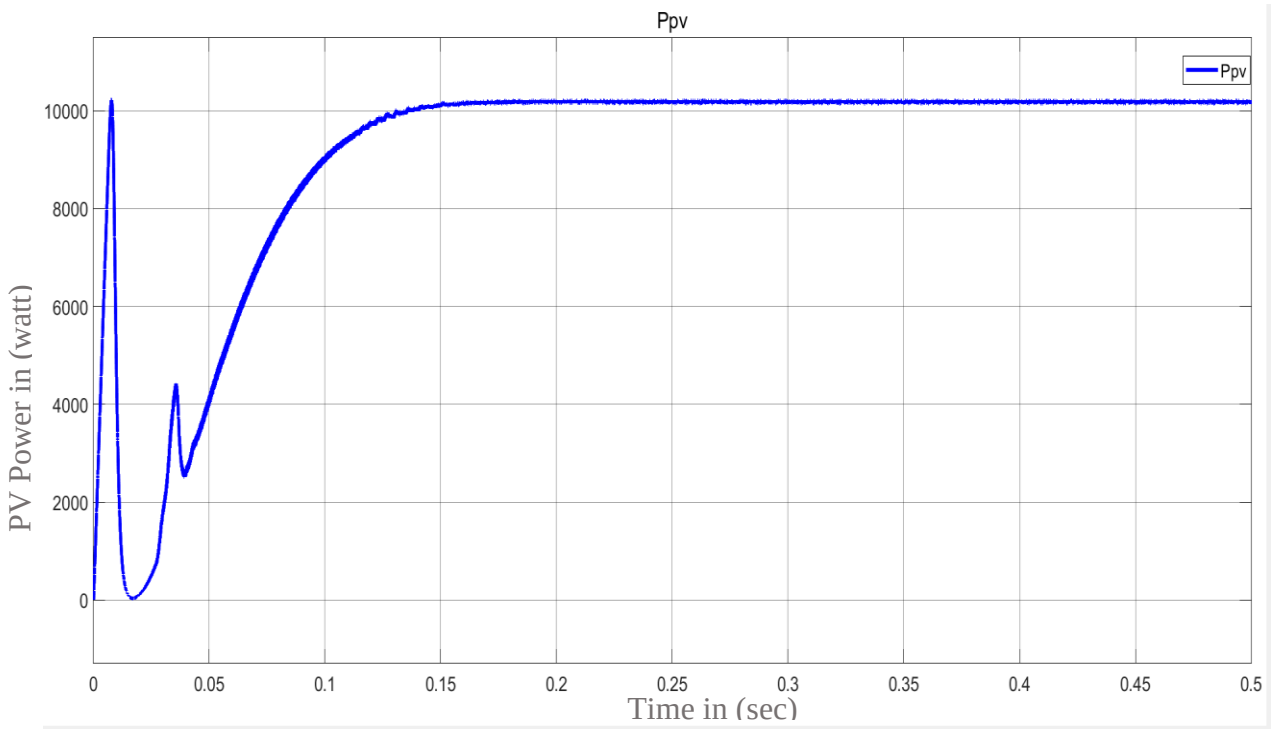

Figure 4. 3: PV Output Power with PI Controller

Figure 4.2 and figure 4.3 above give us the total output power of our PV Array pertaining to the parameters already computed in previous sections. In consideration of the available area and the dimensions of a single PV module, it has been determined that a total of 32 PV panels can be installed on the roof of single train vehicle of the AALRT. With a 320W monocrystalline module (OSMp60-320W), a total power of 10.240kW is expected to be harnessed from the array. Two different scenarios are represented in figure 4.2 and 4.3 respectively. The first graph shows an unstable power curve owning to the flaws of the p/o algorithm. This issue can be handled using a as show in fig. 4.3. The figure gives a smooth PV power curve which has been generated with a PI controller. In both cases, the output power has reached the expected maximum power point value even though the model with PI controller takes a little bit longer: 0.15 sec compared to 0.05 sec of the one with no PI. The PI controller here works by taking the error computed from the comparison of reference voltage and the actual PV voltage. The output of the PI controller then gives a duty cycle of the PWM generation which compared with the carrier signal and given to the IGBT to gives us a better MPPT tracking performance.

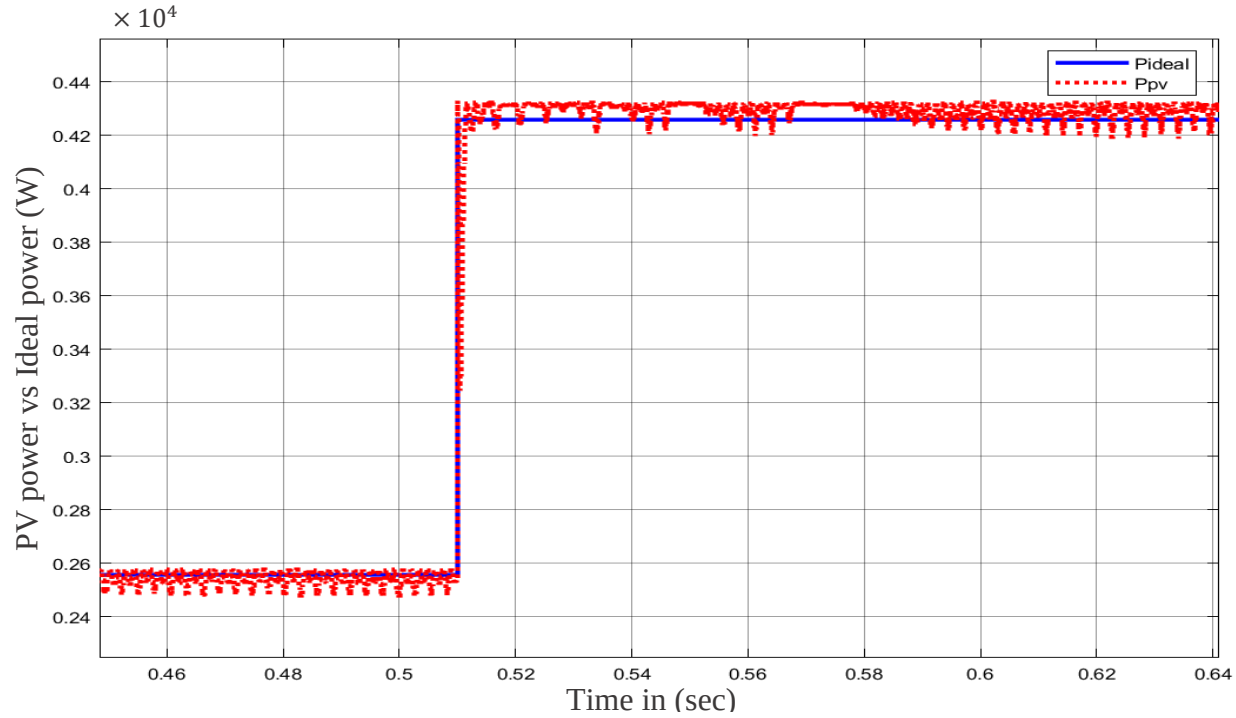

Figure 4. 4: PV Power Fluctuation vs Ideal PV Power

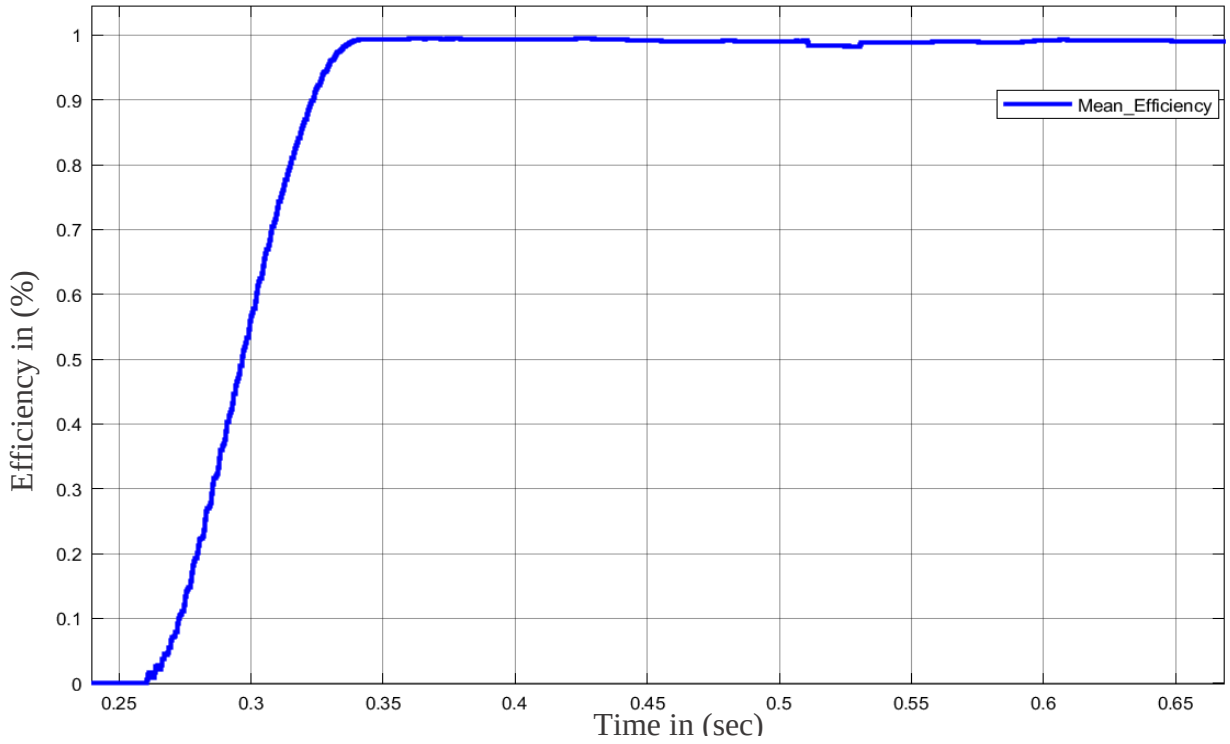

Figure 4. 5: Efficiency of the designed MPPT System

Figures 4.4 and 4.5 are about the MPPT dynamic tracking efficiency calculation of our system. Modern PV-MPPT inverters are now marketed as having a tracking efficiency of up to 99%. While that might be correct in compliance with some standards of measurement, actual energy efficiency over time is always less than what is expected. The inaccuracy of the MPP-tracking is the reason for lower performance of the PV-inverter. This could be significant, particularly in areas with erratic sunlight, which is not frequently encountered in East-Central African countries like Ethiopia. In order to calculate the efficiency of our MPPT algorithm, an ideal power curve has been compared with the actual power curve. As shown in figure 4.5, the mean efficiency has reached a value slightly above 98% which is close to today's marketed MPPT efficiency. The computations were carried out for one particular single variable overcast day, which represents the most extreme, but also the most typical, example of irradiance fluctuations. As a result, the outcomes obtained set the theoretical worst-case limits for perturb and observe tracking efficiency for Ethiopian climate.

4.2 Energy computation and Analysis with Battery Management System

The energy demand-supply analysis is performed here, and the results are summarized in the table 4.1 below.

Table 4. 1:Computation Results

Load Demand in (kWh/d)	Available Energy in (kWh/d)	Battery parameters (Calc.)	PV availability (hrs)	T. Operation Time (Train)	System Availability
$E_a = 128$	$E_{PV} = 68.608$	$T_c = 4hrs$	6.7 hrs	16 hrs	6.7+1.5
	$E_b = 12.62$	$A_b = 1.5hrs$			8.2 hrs

The table above gives us the summary of computation results taking into account all the parameters. The daily energy demand of onboard auxiliary loads has been calculated using equation (18) and found to be 128kWh/train/day. It is worth emphasizing that these calculations were made considering the worst-case scenario due to lack of accurate data on individual loads energy consumption. That means that we have assumed that all auxiliary loads are continuously operational during all the 16 hours (from 6:00 AM to 10:00 PM) of train operation. Therefore, this

amount of energy does not really represent the actual figures of energy consumption since we know that some loads such us door opening control motors, magnetic braking system etc. work at specific time and locations. The available energy from PV system and batteries also has been computed as 68.608kWh/day and 12.62kWh/day respectively as shown in the table 4.1. With the maximum charging current, the battery sets of 100Ah capacity take 4hours to charge while its running time has been calculated as 1.5hours when it is fully relied on. The table also shows the system running time or the system availability which the sum of PV availably and battery availability and this makes up to 8.2 hours of reliance on the designed system.

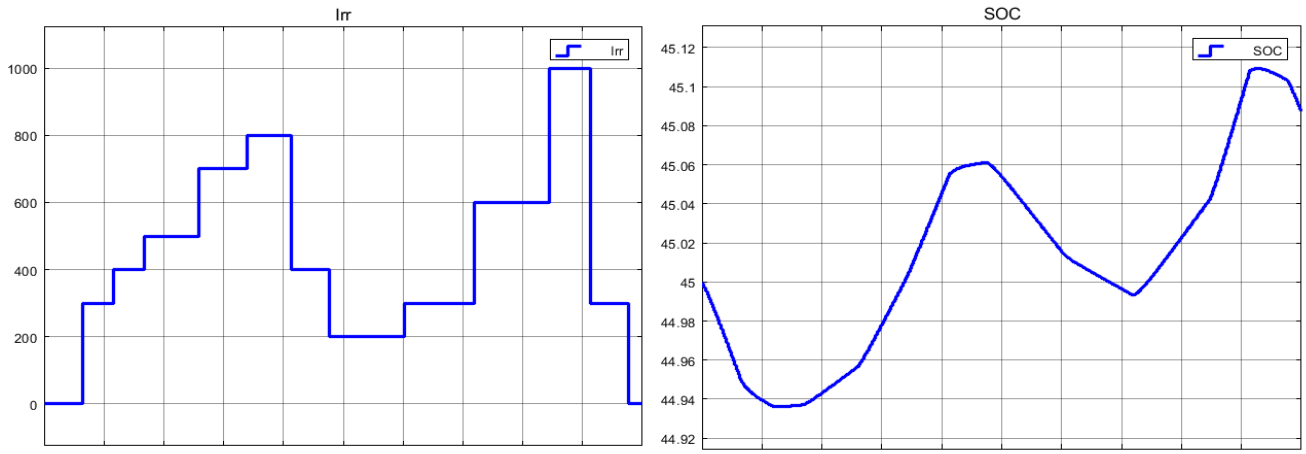

(a) irradiation (b) battery SoC

Figure 4. 6: Battery Charging-Discharging Behavior According to Irradiation

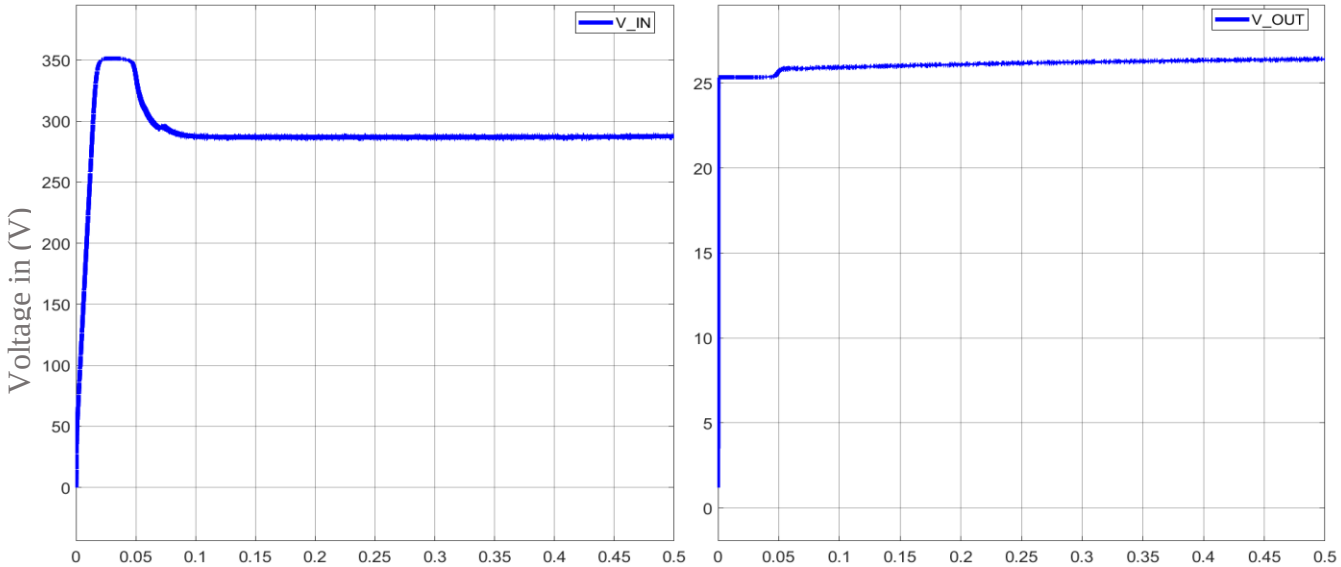

(a) Input Voltage (b) Output Voltage

Figure 4. 7: DC/DC Converter (Buck) Input and Output Voltages

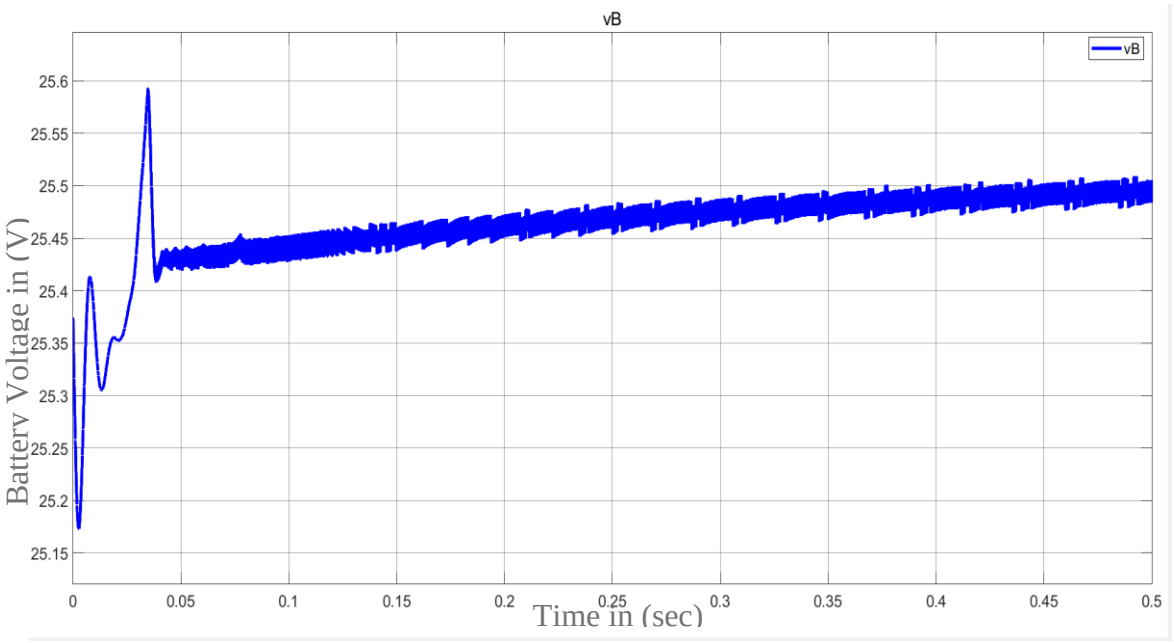

Figure 4. 8: Battery Voltage

Figure 4.6 (a) and (b) shows how the battery respond to irradiation and power fluctuations from the PV panels. The battery sets are linked to the other components through a bi-directional converter because it works in both charging and discharging mode according to the PV power availability. As figure 4.6 shows, the battery state of charge curve follows the irradiation fluctuations. This is because the irradiation dictates the PV output power and the later dictate the battery behavior. We can observe that, when irradiation is from 0 to 300 (figure 4.6 (a)), the battery is in discharging (figure 4.6 (b)) since the PV array is not generating enough power to feed the loads. The battery starts charging with a slow charging rate when the irradiation reaches around 400. It continues charging and increasing the charging rate as the irradiation increases until it falls again. The battery set behave in this way through a developed battery Energy Management System (EMS) algorithm that considers solar array output power $\mathbf{P_{pv}}$, the battery energy storage power $\mathbf{P_{battery}}$, the battery state of charge **SOC**, the total auxiliary $\mathbf{P_{load}}$ and the auxiliary power supply power $\mathbf{P_{APS}}$, then perform the energy management described in section 3.3. Figure 4.7 (a) and (b) illustrate the voltages at the input and output of the DC/DC buck converter, respectively. The back converter has been used here to control and step down the high input voltage (250V-320V) from the PV array to the low voltage (24V-29V) suitable for DC loads and batteries charging as depicted from the figures. The output voltage from the buck converter is around 25.5V and the same voltage level is supplied to the batteries for charging as seen in figure 4.8.

4.3 Economic Analysis of the Proposed System

As we already described in the section 3.4 of this work, the payback period technique has been used to evaluate the system profitability and its economic impact. Equation (24) has been used to this end. With respect to actual cost on amazon, the initial investment cost for PV and MPPT has been calculated at the rate of $0.22/Wp and $700, respectively. For 32 PV panels of 320Wp each, the total cost is $2,252.8 while the MPPT price remains the same for we need only one. This makes the investment cost up to $2,952.8 multiplied by the number of train vehicle of the AALRT which raise the total initial investment cost to $121, 064.8. On the other hand, the electricity tariffs in Ethiopia stand at $0.06/kWh. Information from table 4.1 gives us a total amount of energy provided by our PV and battery system which is 81.228kWh/train/day. For the 41 train vehicles, by multiplying with the energy saved per train, the total energy saved is around 3.33MWh/day, and this translate to $199.82/day. Therefore, the cash inflow per year is calculated and found to be $72,934.3. The payback period is therefore computed using equation (24) and it is found as 1.7 years which is around **20 moths.**

4.4 Shading Impact Analysis

Since the solar panels elements are sensitive areas, they are managed differently by the program, solar panels cannot be incorporated into building objects. They must be placed on the main 3D scene's buildings. The irradiance reduction is generally determined for the PV array area when forecasting the yield, as detailed in section 3.8 of the methodology. However, this neglects to account for the fact that shading alters the PV array's distinctive I-V curve. The amount of energy lost depends on how long the shading lasts throughout the day/year.

As depicted in figures 4.9 and 4.10 two locations with potential high shading impact have been identified and simulated using PVSyst software. This study has considered the coordinates of these locations in the computation of the results. The first case considered the **wegagen bank building** situated around stadium at 9º0’42.72” N latitude and 38º45’20.43” E Longitude as shadow-cast object. The resulting shading loss is illustrated in figure 31 (a) with a relatively low value of 0.8%. as shown in figure 4.11 The second scenario considered the **capital hotel** situated around hayahulet at 9º0’47.85” N latitude and 38º46’46.66” E Longitude. The resulting shading loss has been computed as 1.3%. It is worth noticing that the losses are low for both cases, this is due to the fact

that there is enough clearance from the track to the building. The case around stadium registered an even lower shading loss because the train itself is elevated which reduces the impact of shadow.

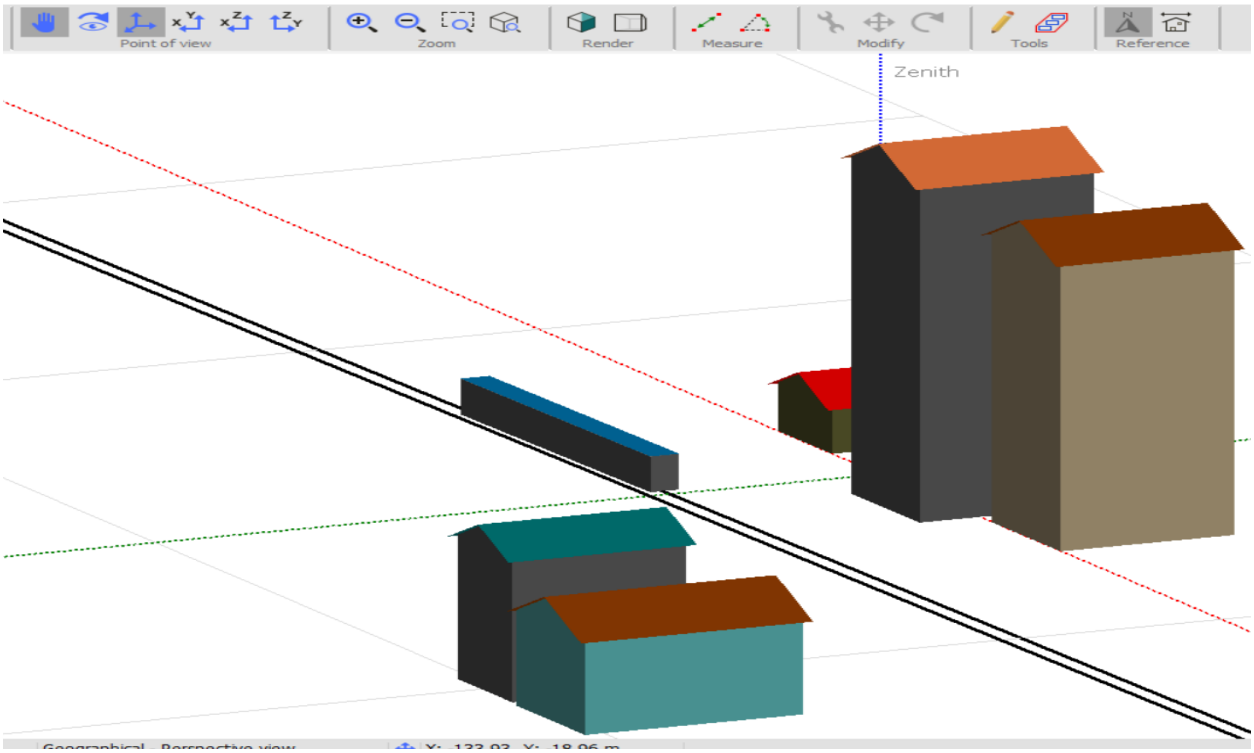

Figure 4. 9: Shading Situation Around Stadium (Wegagen Bank)

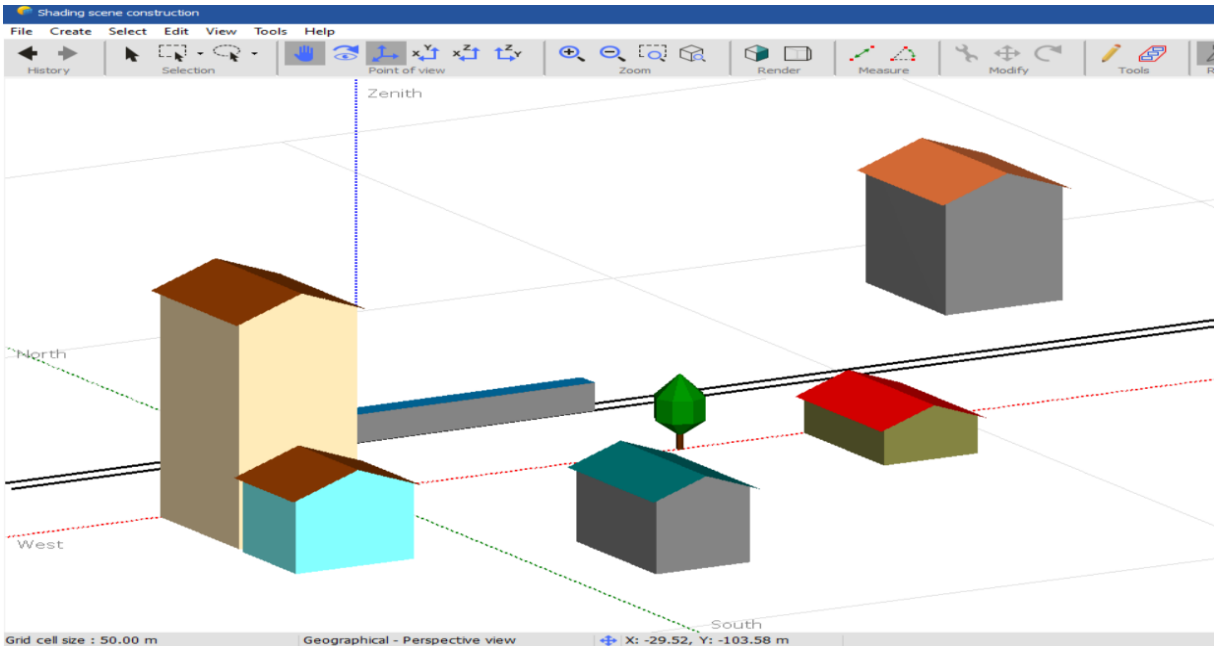

Figure 4. 10:Shading Situation Around Hayahulet (Capital hotel)

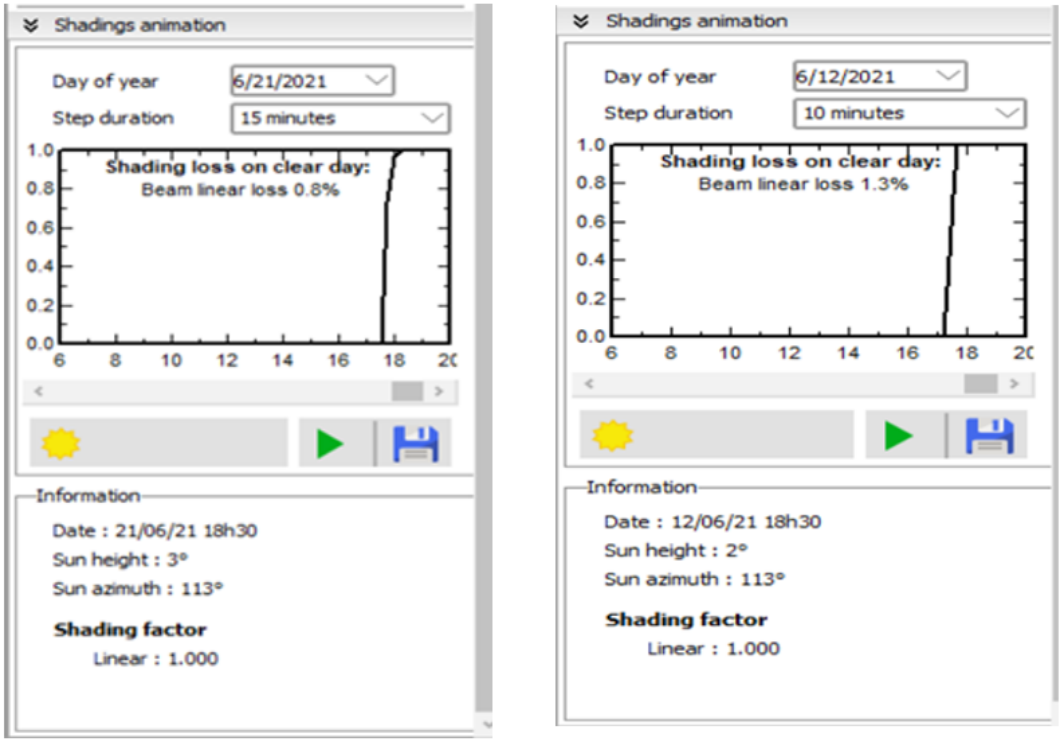

(a) Around Stadium

(b) Around Hayahulet

Figure 4. 11: Shading losses

It should be noted that this research took the worst-case situation into account. Because the software we are using does not have tools for evaluating moving PV arrays, the train is considered stationary. We can therefore conclude that the effect of the shadow is negligible even in the worst-case scenario for the proposed system.

4.5 Regenerative Energy for Other High Energy Consuming AC auxiliary Loads

The regenerative braking energy could be utilized to deliver power the heavy energy consumer auxiliary loads such as air conditioning system which was left out of our PV system designing due to its high-power demand. From the results in table 4.2 below, when the train is running at the speed above the average speed, it results in generating a higher energy during braking period. Contrary to the energy consumption, the train consumes a bit higher energy when it is running at higher speed. While low energy consumption is observed for the speed below the average speed.

Table 4. 2: Regenerated Energy for Both direction of East-West line

Interstation	**Forward direction**		**Return direction**	
	E reg at Max. Speed(KWh)	**Ereg at Aver. speed(KWh)**	**Ereg at Max. Speed(KWh)**	**Ereg at Aver. speed(KWh)**
Torhailoch-Cocacola	1.73	0.198	2.401	0.276
Cocacola-Lideta	2.526	0.292	2.398	0.278
Lideta-Tegbared	2.529	0.292	2.401	0.277
Tegbared-Mexico Square	3.102	0.359	2.399	0.279
Mexico Square-Leghar	3.213	0.372	2.395	0.277
Leghar-Stadium	1.534	0.177	2.401	0.281
Stadium-Esthephanos	2.529	0.292	2.398	0.277
Esthephanos-Bambis Hotel	2.526	0.292	2.394	0.287
Bambis Hotel-St-Urael	2.533	0.293	2.396	0.267
St.Urael-Hayahullet2	3.12	0.361	2.221	0.257
Hayahullet2-Hayahullet1	2.706	0.313	1.807	0.208
Hayahullet1-Lem Hotel	2.53	0.293	2.394	0.277
Lem Hotel-Meganagna	2.517	0.293	2.401	0.277
Meganagna-Gurdashola2	2.529	0.292	2.398	0.277
Gurdshola2-Gurdashola1	2.526	0.292	3.393	0.393
Gurdshla1-Mgt.Institute	2.531	0.293	3.082	0.357
Mgt.Institute-C.S.College	2.528	0.292	1.825	0.211
C.S.College-St-Michael	2.526	0.292	2.398	0.277
St.Michael-CMC	2.529	0.292	2.401	0.278
CMC-Meri	2.526	0.292	3.206	0.371
Meri-Ayat	2.526	0.292	2.4	0.277
Total	**53.317**	**6.166**	**51.62**	**5.953**

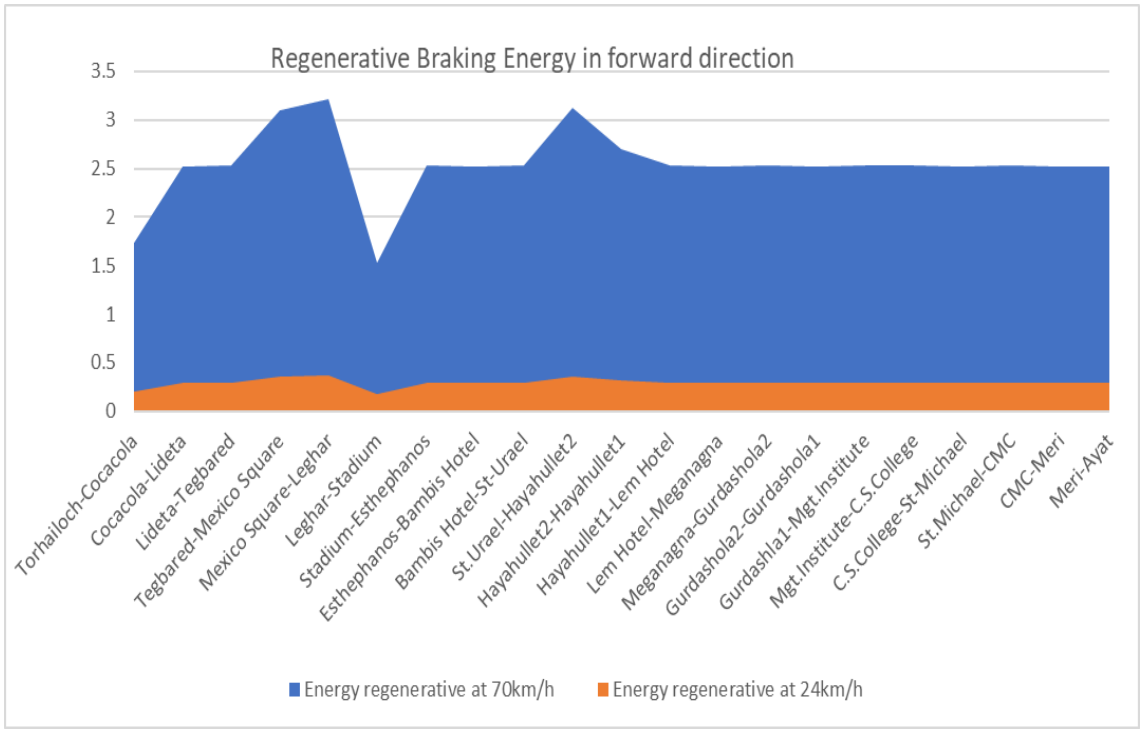

Figure 4. 12: Regenerative Braking Energy in Forward Direction E-W line

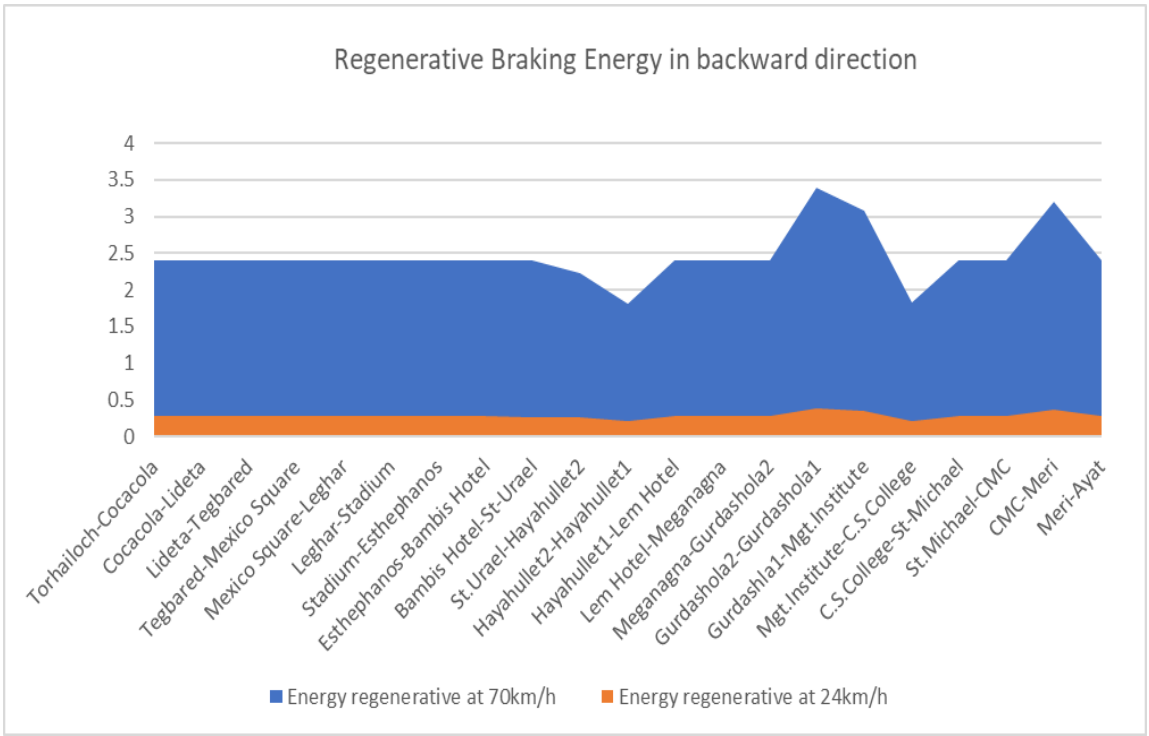

Figure 4. 13: Regenerative Braking Energy in Forward Direction E-W line

Figures 4.12 and 4.13 present the variations of regenerative braking energy in forward and return direction, respectively. From these figures we can realize that the train generates higher energy during braking period when running at the speed above the average. A relatively high energy consumption is also observed with this high speed whereas low energy consumption is observed for the speed below the average.

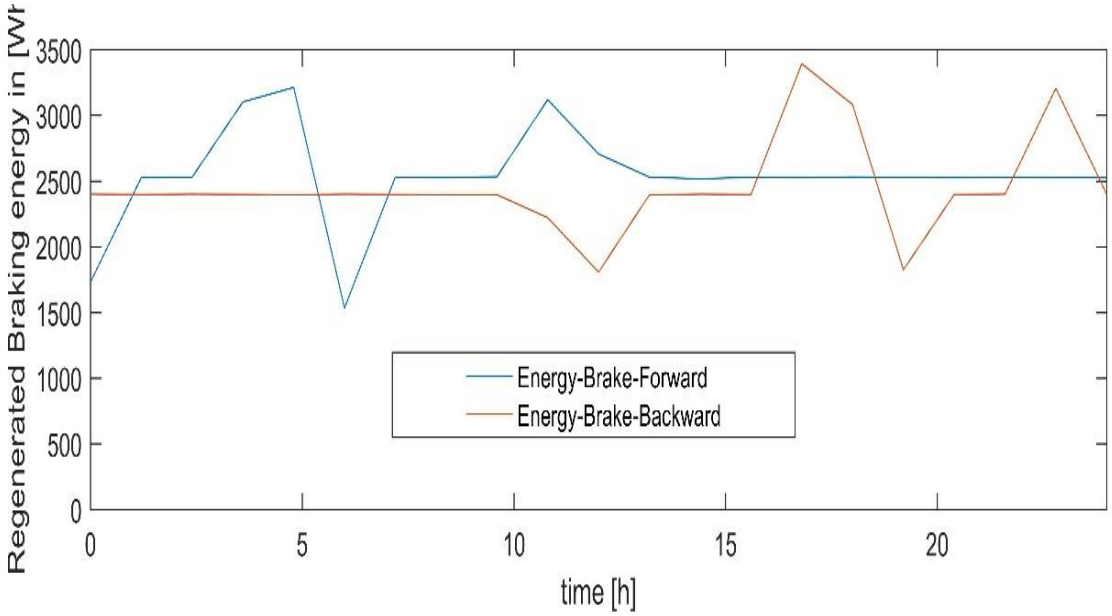

Figure 4. 14: Regenerative Energy from Braking for Est-West Line

Figure 4.14 portrays the regenerative energy from braking, both forward and Return. We can realize from this figure that the area covered by the curves in both forward and Return directions are approximately the same. This may lead us to conclude that the energy regenerated from the braking system are almost equal. However, a slight difference materialized by a surplus production in average for the forward direction can be noticed. Note also that the energy from braking present less fluctuations and that helps to keep the system in a more stable and predictable mode.

So far, the energy consumption and regenerative have been computed by considering one-way trip for the train. The AALRT has in average fourteen trips per day (seven forward and seven return trips regularly).

CHAPTER 5: CONCLUSIONS AND RECOMMENDATIONS

5.1 Conclusions

Ethiopia, as we all know, is located in the equatorial zone, where the sun shines brightly virtually all year and has the ability to generate a lot of energy. The primary purpose of this research was to suggest an effective photovoltaic and energy storage integration method for light weight train auxiliary loads focusing on the Addis Ababa Light Rail Transit (AALRT) as a case of study. This was accomplished through comprehensive designs and simulations considering different parameters. The effective available area on the train roof has been determined first since it is a fixed parameter. Mathematical evaluations have proven that the roof can accommodate a total number of 32 PV panels of monocrystalline module type, model OSMp60-320W. The energy requirement study was carried out in order to gain a precise understanding of the train's auxiliary energy usage in order to reduce energy consumption while maintaining proper functioning. To provide quantifiable estimates of electricity load consumption, an auxiliary load inventory was conducted. These calculations were crucial in determining the type and size of our PV and battery storage system.

The maximum power point tracking system with the perturb and observe algorithm has been used to track the PV power to a total of around 10.24kW. MPPT has been implemented with and without a PI controller and the results analysis has demonstrated that the PI controller helps to smoothen the curve, but at the expense of a delay compared to the system without PI controller. The efficiency of our MPPT was around 98%. A DC/DC converter of the type back has been designed to control and step down the high input voltage from the PV array to the low voltage (24-29V) suitable for DC loads and batteries charging. The energy demand-supply analysis has also been carried out to evaluate the system availability. The results have shown that the PV energy combined with the battery energy can supply the onboard auxiliary loads for 8.2 hours. It has also been demonstrated that the proposed PV system helps to save around 82.228kWh/train/day which makes up to 3.33MWh/day for the total number of train vehicle on the AALRT. An economic evaluation of the system has been carried out to justify its adoption. The payback period approach has been used to assess the effectiveness of placing a PV array on the train roof for the proposed system and it was found that with a cash inflow of $199.82/day, the system would pay back its investment within around 20 months.

The influence of shadows on the moving panels mounted on the railcar's roof was captured via shading analysis. PVsyst software was used to accomplish this, which is based on metrological data imported from the program database. Along the rail track, Google Earth software was utilized to identify sites with a high potential for shading impact. The simulations for the two identified sites returned a shading loss of 0.8% and 1.3% considering the worst-case scenario (train not moving). From this, we have concluded that the shading impact is negligible for the consider E-W line.

Regenerative braking energy has also been modelled and evaluated for a possibility of supplying the AC auxiliary loads that require high energy beyond the PV capacity such as the air conditioning system. For the considered E-W line as a case study for this, it has been determined that Average daily regenerative braking energy is high enough to be used on auxiliary loads. The details on how to supply the AC loads with the regenerative braking energy remain to be studied for future work.

5.2 Limitations and Recommendations

Because of various constraints that this research was conducted under, it necessitates a more in-depth investigation. Owing to lack of sufficient data on the energy consumption and schedule of individual loads , this study considered the worst-case scenario that all auxiliary loads are operating all the time. However, some loads such as door opening control motors, magnetic braking system work in particular situations. This study did not take into account the impact of extra PV weight on the train traction energy consumption as it only focused on the auxiliary energy consumption not the traction energy consumption. The shading analysis in this study did not consider neither the movement of the train nor the semi-underground on the N-S line around Piassa. Finally, the scope of this study was limited to regenerative braking energy modelling but did not study the details of how to connect to the ac conditioning unit.

As a result, the following future works have been suggested:

1. An in-depth collection and analysis of data on the energy consumption of individual auxiliary loads and their operation time should be studied.
2. The shadow analysis of the semi-underground (Piassa) and the moving panels should be carefully studied.
3. Details on regenerative braking usage to supply other high-power loads such as ac conditioning system, escalators, elevators etc. need an in-depth study.

References

[1] G. Graber, V. Calderaro, V. Galdi, A. Piccolo, R. Lamedica, and A. Ruvio, "Techno-economic sizing of auxiliary-battery-based substations in DC railway systems," *IEEE Trans. Transp. Electrif.*, vol. 4, no. 2, pp. 616–625, 2018, doi: 10.1109/TTE.2018.2825651.

[2] A. González-Gil, R. Palacin, and P. Batty, "Sustainable urban rail systems: Strategies and technologies for optimal management of regenerative braking energy," *Energy Convers. Manag.*, vol. 75, pp. 374–388, 2013, doi: 10.1016/j.enconman.2013.06.039.

[3] F. Ciccarelli, L. P. Di Noia, and R. Rizzo, "Integration of photovoltaic plants and supercapacitors in tramway power systems," *Energies*, vol. 11, no. 2, pp. 1–14, 2018, doi: 10.3390/en11020410.

[4] G. K. G, "SOLAR TRAIN," *Dep. Electron. Commun.*, vol. 6, no. 2, 2016.

[5] M. Lencwe, S. D. Chowdhury, and H. M. Elgohary, "Solar Photovoltaic Integration on Locomotive Roof Top for South African Railway Industry," *Conf. proceedings, IEEE*, no. May 2019, 2016, doi: 10.1109/UPEC.2016.8114087.

[6] M. Spiryagin, Q. Wu, P. Wolfs, Y. Sun, and C. Cole, "Comparison of locomotive energy storage systems for heavy-haul operation," *Int. J. Rail Transp.*, vol. 00, no. 00, pp. 1–15, 2017, doi: 10.1080/23248378.2017.1325719.

[7] N. B. Leo Murray, *Powering our railways with Solar PV*. 2017.

[8] N. George and S. Daniel Chowdhury, "Roof-Top Solar Power Augmentation to Auxiliary Supply of Passenger Train," *2018 IEEE PES/IAS PowerAfrica, PowerAfrica 2018*, no. 2, pp. 793–798, 2018, doi: 10.1109/PowerAfrica.2018.8521156.

[9] N. Regis, "Optimal Battery Sizing of a Grid-Connected Residential Photovoltaic System for Cost Minimization using PSO Algorithm," *Eng. Technol. Appl. Sci. Res.*, vol. 9, no. 6, pp. 4905–4911, 2019, doi: 10.48084/etasr.3094.

[10] P. Gouthami, R. Dana, P. Elisa, B. B. Koo, K. Sandra, and F. Gina, "Beyond Connections: Energy Access Diagnostic Report Based on the Multi-Tier Framework," *Int. Bank Reconstr. Dev. / World Bank*, 2018, doi: 10.1596/24368.

[11] M. A. Ocklenburg, M. Dohmen, X. Q. Wu, and M. Helsper, "Next generation DC-DC converters for Auxiliary Power Supplies with SiC MOSFETs," *2018 IEEE Int. Conf. Electr. Syst. Aircraft, Railw. Sh. Propuls. Road Veh. Int. Transp. Electrif. Conf. ESARS-ITEC 2018*, 2019, doi: 10.1109/ESARS-ITEC.2018.8607463.

[12] L. Zhang, L. Yun, M. Sun, and B. Peng, "Simulation research on auxiliary power supply system of china standard EMU," *Electron.*, vol. 8, no. 6, 2019, doi: 10.3390/electronics8060647.

[13] Y. Wang, W. Liu, T. Wang, X. Liu, Z. Chen, and Z. Yang, "Research on the modularization

of the auxiliary power supply system of the high-speed train," *ITEC Asia-Pacific*, vol. 377, pp. 461–472, 2016, doi: 10.1007/978-3-662-49367-0_47.

[14] I. Quesada *et al.*, "Modulation technique for low frequency harmonic cancellation in auxiliary railway power supplies," *IEEE Trans. Ind. Electron.*, vol. 58, no. 9, pp. 3976–3987, 2011, doi: 10.1109/TIE.2010.2102320.

[15] I.-H. C.-M. J.-H. Lee, "Research on High-Efficiency Power Conversion Structure for Railroad Auxiliary Power Supply(APS) System," *J. KOREAN Soc. Railw.*, vol. 19, no. 3, pp. 297–303, 2016, doi: 10.13335/j.1000-3673.pst.2017.1709.

[16] L. S. Xavier, W. C. S. Amorim, A. F. Cupertino, V. F. Mendes, W. C. do Boaventura, and H. A. Pereira, "Power converters for battery energy storage systems connected to medium voltage systems: a comprehensive review," *BMC Energy*, vol. 1, no. 1, pp. 1–16, 2019, doi: 10.1186/s42500-019-0006-5.

[17] L. Jia, J. Ma, S. Member, P. Cheng, and Y. Liu, "A Perspective on Solar Energy-powered Road and Rail Transportation in China," *IEEE J. POWER ENERGY Syst.*, vol. 6, no. 4, pp. 760–771, 2020, doi: 10.17775/CSEEJPES.2020.02040.

[18] N. Uddin, M. M. Rashid, M. A. Aziz, and N. A. Nithe, "Maximum power point charge controller for DC-DC power conversion in solar PV System," *Glob. J. Res. Eng.*, vol. 16, no. 1, 2016.

[19] B. J. Yoo, C. B. Park, and J. Lee, "A study on design of photovoltaic system using electrical railway stations," *19th Int. Conf. Electr. Mach. Syst. ICEMS 2016*, 2017.

[20] A. DOLARA, R. FARANDA, and S. LEVA, "Energy Comparison of Seven MPPT Techniques for PV Systems," *J. Electromagn. Anal. Appl.*, vol. 01, no. 03, pp. 152–162, 2009, doi: 10.4236/jemaa.2009.13024.

[21] A. Pandey and D. K. Singh, "A Review of Modelling of Photovolaic Solar Cell for Maximum Power Point Tracking," *Int. J. Sci. Res.*, vol. 5, no. 4, pp. 2462–2464, 2016, doi: 10.21275/v5i4.nov163163.

[22] S. Venugopal, A. S. Aspalli, and R. Raveendra, "Maximum Power Point Tracking For Photovoltaic Systems," *Proc. Int. Conf. Curr. Trends Eng., Sci. Technol. ICCTEST*, no. December, pp. 432–441, 2017, doi: 10.21647/icctest/2017/49002.

[23] R. Sridhar, S. Jeevananthan, N. T. Selvan, and S. Chowdary, "Performance improvement of a photo voltaic array using MPPT (P&O) technique," *2010 IEEE Int. Conf. Commun. Control Comput. Technol. ICCCCT 2010*, pp. 191–195, 2010, doi: 10.1109/ICCCCT.2010.5670550.

[24] X. Liu and L. A. C. Lopes, "An improved perturbation and observation maximum power point tracking algorithm for PV arrays," *PESC Rec. - IEEE Annu. Power Electron. Spec. Conf.*, vol. 3, pp. 2005–2010, 2004, doi: 10.1109/PESC.2004.1355425.

[25] P. Wang, H. Ding, C. Diao, and S. Qi, “An improved MPPT algorithm based on traditional incremental conductance method,” *2011 4th Int. Conf. Power Electron. Syst. Appl. PESA 2011*, no. 2, pp. 3–6, 2011, doi: 10.1109/PESA.2011.5982914.

[26] K. A. Aganah and A. W. Leedy, “A constant voltage maximum power point tracking method for solar powered systems,” *Proc. Annu. Southeast. Symp. Syst. Theory*, pp. 125–130, 2011, doi: 10.1109/SSST.2011.5753790.

[27] R. Ramaprabha, V. Gothandaraman, K. Kanimozhi, R. Divya, and B. L. Mathur, “Maximum power point tracking using GA-optimized artificial neural network for solar PV system,” *2011 1st Int. Conf. Electr. Energy Syst. ICEES 2011*, no. 1, pp. 264–268, 2011, doi: 10.1109/ICEES.2011.5725340.

[28] K. Ishaque, Z. Salam, M. Amjad, and S. Mekhilef, “An improved particle swarm optimization (PSO)-based MPPT for PV with reduced steady-state oscillation,” *IEEE Trans. Power Electron.*, vol. 27, no. 8, pp. 3627–3638, 2012, doi: 10.1109/TPEL.2012.2185713.

[29] F. Nadeem, S. M. S. Hussain, P. K. Tiwari, A. K. Goswami, and T. S. Ustun, “Comparative review of energy storage systems, their roles, and impacts on future power systems,” *IEEE Access*, vol. 7, pp. 4555–4585, 2019, doi: 10.1109/ACCESS.2018.2888497.

[30] X. Luo, J. Wang, M. Dooner, and J. Clarke, “Overview of current development in electrical energy storage technologies and the application potential in power system operation,” *Appl. Energy*, vol. 137, pp. 511–536, 2015, doi: 10.1016/j.apenergy.2014.09.081.

[31] J. Campillo, N. Ghaviha, N. Zimmerman, and E. Dahlquist, “Flow batteries use potential in heavy vehicles,” *Electr. Syst. Aircraft, Railw. Sh. Propulsion, ESARS*, vol. 2015-May, pp. 1–6, 2015, doi: 10.1109/ESARS.2015.7101496.

[32] M. Khodaparastan, A. A. Mohamed, and W. Brandauer, “Recuperation of regenerative braking energy in electric rail transit systems,” *IEEE Trans. Intell. Transp. Syst.*, vol. 20, no. 8, pp. 2831–2847, 2019, doi: 10.1109/TITS.2018.2886809.

[33] P. Radcliffe, J. S. Wallace, and L. H. Shu, “Stationary applications of energy storage technologies for transit systems,” *EPEC 2010 - IEEE Electr. Power Energy Conf. “Sustainable Energy an Intell. Grid,”* no. 1, 2010, doi: 10.1109/EPEC.2010.5697222.

[34] E. Steve, “Long Island bus NaS battery energy storage project-EPRI,” *DOE Peer Rev. Energy Storage Power Electron. Syst. Res. Program,Seattle,WA*, no. 704, 2009, [Online]. Available: http://www.sandia.gov/ess/docs/pr_conferences/2009/eckroad.pdf.

[35] Y. Kishinevsky, “Long Island Bus Sodium Sulfur (NaS) Battery Storage Project,” *Eesat*, 2005.

[36] M. Khodaparastan, A. A. Mohamed, and W. Brandauer, “Recuperation of regenerative braking energy in electric rail transit systems,” *IEEE Trans. Intell. Transp. Syst.*, vol. 20, no. 8, pp. 2831–2847, 2019, doi: 10.1109/TITS.2018.2886809.

[37] A. G. Vidhya K Viswambharan, Vijaya Kumar, Kainat Amjad, “A Case Study- Solar Powered Metro in UAE,” *2018 5th Int. Conf. Renew. Energy Gener. Appl.*, vol. 1, pp. 46–51, 2018.

[38] J. A. Aguado, A. J. S. Racero, and S. De La Torre, “Optimal operation of electric railways with renewable energy and electric storage systems,” *IEEE Trans. Smart Grid*, vol. 9, no. 2, pp. 993–1001, 2018, doi: 10.1109/TSG.2016.2574200.

[39] M. A. Wei and W. Wei, “Auxiliary power supply system of passenger train based on photovoltaic and energy storage,” *IEEE 11th Conf. Ind. Electron. Appl.*, vol. 6, no. 2, pp. 784–788, 2016.

[40] M. J. Lencwe, S. P. Chowdhury, and H. M. Elgohary, “Solar photovoltaic integration on locomotive roof top for South African railway industry,” *Proc. - 2016 51st Int. Univ. Power Eng. Conf. UPEC 2016*, vol. 2017-Janua, pp. 1–5, 2016, doi: 10.1109/UPEC.2016.8114087.

[41] L. Jian and C. Min, “Application of solar PV grid-connected power generation system in Shanghai rail transit,” *China Int. Conf. Electr. Distrib. CICED*, no. 201802280000037, pp. 110–113, 2018, doi: 10.1109/CICED.2018.8592209.

[42] S. Elisabeta, P. Bogdan, P. Ion, N. Valentin, and P. Florina, “Use of Renewable Energy Sources to Power Railroad Traffic Safety Installations,” *2019 11th Int. Symp. Adv. Top. Electr. Eng. ATEE 2019*, pp. 1–4, 2019, doi: 10.1109/ATEE.2019.8724999.

[43] S. K. Bade and V. Kulkarni, “Use of Renewable energy in performance enhancement of Indian Traction Power Supply System,” *Proc. - 2018 Int. Conf. Smart Electr. Drives Power Syst. ICSEDPS 2018*, pp. 111–116, 2018, doi: 10.1109/ICSEDPS.2018.8536056.

[44] O. Perpiñan, E. Lorenzo, and M. A. Castro, “On the calculation of energy produced by a PV grid-connected system,” *Prog. Photovoltaics Res. Appl.*, vol. 15, no. 3, pp. 265–274, 2007, doi: 10.1002/pip.728.

[45] M. N. Dehedkar and P. S. Vitthalrao Murkute, “Optimization of PV system using distributed MPPT control,” *Proc. 2018 Int. Conf. Syst. Model. Adv. Res. Trends, SMART 2018*, pp. 216–220, 2018, doi: 10.1109/SYSMART.2018.8746931.

[46] M. S. Kaltiya, M. S. Abubakar, and I. N. Itodo, “Open Access Prediction of Global Solar Radiation Using Angstrom-Page Equation Model for Makurdi Benue State , Nigeria,” *Am. J. Eng. Res.*, vol. 03, no. 08, pp. 145–150, 2014.

[47] A. Razmjoo, S. M. Heibati, and M. Ghadimi, “Using Angstrom-Prescott (A-P) Method for Estimating Monthly Global Solar Radiation in Kashan,” *J. Fundam. Renew. Energy Appl.*, vol. 6, no. 5, 2016, doi: 10.4172/2090-4541.1000214.

[48] A. O. Onyango and V. Ongoma, “Estimation of mean monthly global solar radiation using sunshine hours for Nairobi City, Kenya,” *J. Renew. Sustain. Energy*, vol. 7, no. 5, 2015, doi: 10.1063/1.4930530.

[49] E. Chang, “MODELS FOR ESTIMATING ENERGY CONSUMPTION OF,” *J. East. Asia Soc. Transp. Stud.*, vol. 6, no. May, pp. 278–291, 2014, doi: 10.11175/easts.6.278.

[50] K. Yang and Y. Tang, “Parameter Identification and State-of-Charge Estimation for Lithium-Ion Batteries Using Separated Time Scales and Extended Kalman Filter,” *MDPI, Energies*, vol. 14, no. 1054, 2021.

[51] W. Xiong, Y. Mo, and C. Yan, “Lithium-Ion Battery Parameters and State of Charge Joint Estimation Using Bias Compensation Least Squares and the Alternate Algorithm,” *Hindawi Math. Probl. Eng.*, vol. 2020, 2020.

[52] M. H. RASHID, *POWER ELECTRONICS Academic Press Series in Engineering*. 2001.

[53] M. Zeraatpisheh, R. Arababadi, and M. S. Pour, “Economic analysis for residential solar PV systems based on different demand charge tariffs,” *Energies*, vol. 11, no. 12, 2018, doi: 10.3390/en11123271.

[54] M. Khodaparastan, S. Member, A. Mohamed, and S. Member, “Modeling and Simulation of Regenerative Braking Energy in DC Electric Rail Systems,” *2018 IEEE Transp. Electrif. Conf. Expo*, no. June, pp. 1–6, 2018, doi: 10.1109/ITEC.2018.8450133.

[55] M. Khodaparastan, S. Member, A. A. Mohamed, S. Member, and W. Brandauer, “Recuperation of Regenerative Braking Energy in Electric Rail Transit Systems,” *IEEE Trans. Intell. Transp. Syst.*, vol. 7, pp. 1–16, 2018.

Appendix A: Main Circuit Diagram of the Auxiliary Power Box of the AALRT

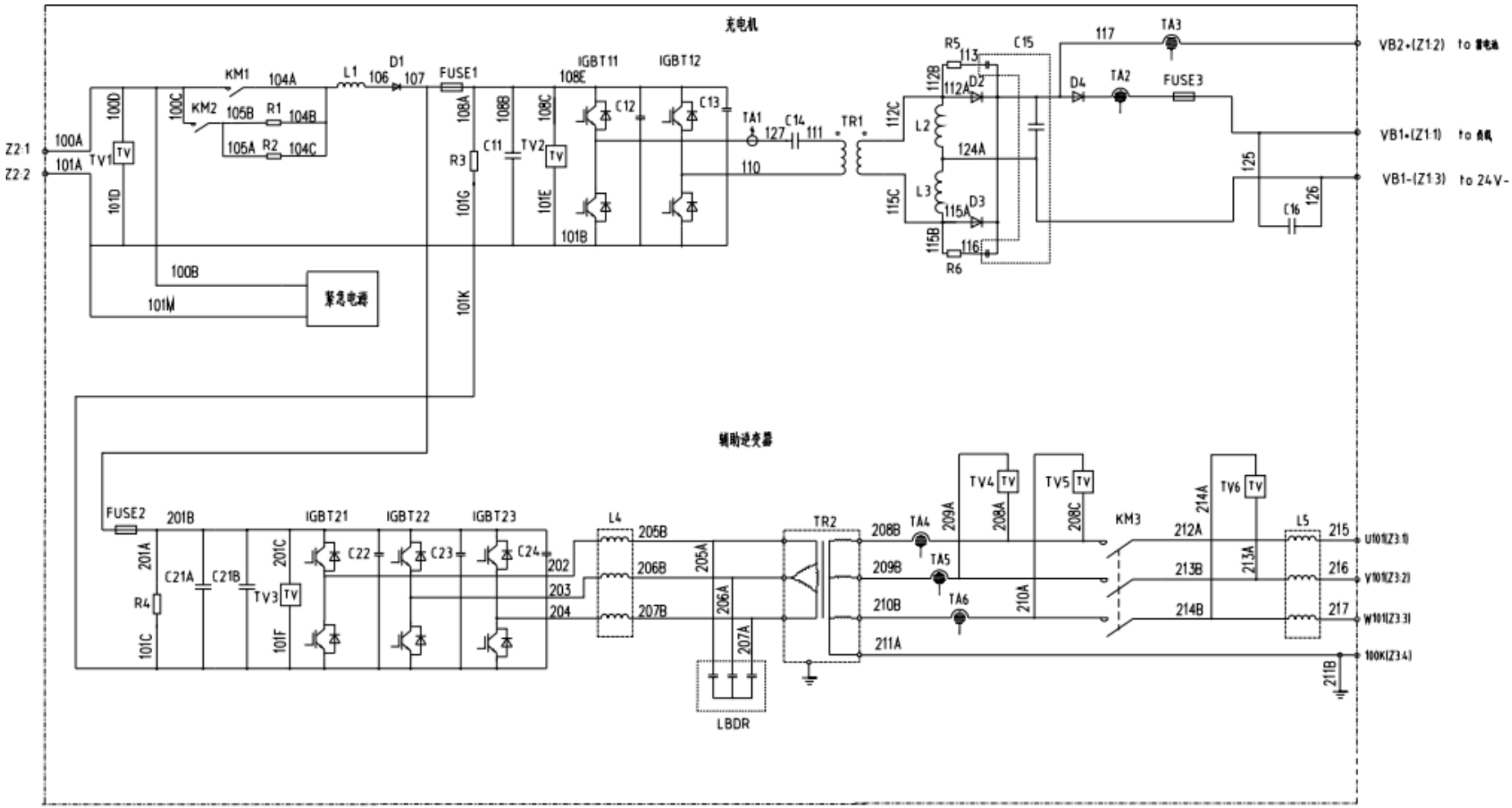

In the upper part of the figure above is the charger, and in the lower part is the auxiliary inverter. The auxiliary inverter and charger share the EMI input filter, contactor and inlet wire reactance. The supporting capacitor of the charger is in parallel connection with the supporting capacitor of the auxiliary inverter.

The charger adopts the control mode of full-bridge phase-shift zero-voltage soft switching, the switch frequency of which is 20KHz. It is composed of a bridge inverter, a high-frequency transformer, a secondary current double rectifier and an output filter.

As shown in figure, the bridge inverter is composed of two IGBT modules (IGBT11, IGBT12), accompanied by a resonant capacitor and a resonant inductance (achieved by leakage inductance of high-frequency transformer). Zero-voltage turn-on and turn-off of the IGBT is achieved through a resonant process induced by the resonant capacitor and the resonant inductance, thereby reducing the switching loss of the power elements. The efficiency of the charger is ≥85%, and rectification is achieved by means of a current double rectifier.

The auxiliary inverter adopts the working mode of SVPWM (voltage space-vector pulse-width modulation) and its IGBT turn-on and turn-off frequency is 4KHz. The DC input voltage is inverted into a three-phase PWM wave through a three-phase Inverter Bridge. And then the PWM wave is filtered by the LC sinusoidal filter into a three-phase sinusoidal output voltage waveform with harmonic contents less than 5%. Since it is required out of safety consideration that the input and output be electrically isolated from each other, a 35KVA three-phase power-frequency transformer is added to the output side. The connection group of the power-frequency transformer is Dyn11. There is output at the output neutral point, which provides single-phase 220V power supply to a part of the single-phase load.

Appendix B: MPPT Algorithm Code

```
function Vref = RefGen(V,I)
Vrefmax=361;
Vrefmin=300;
Vrefinit=287;
deltaVref=1;
persistent Vold Pold Vrefold;

dataType='double';
if isempty(Vold)
    Vold=0;
    Pold=0;
    Vrefold=Vrefinit;
end
P=V*I;
dV=V-Vold;
dP=P-Pold;
if dP~=0
    if dP<0
        if dV<0
            Vref=Vrefold+deltaVref;
        else
            Vref=Vrefold-deltaVref;
        end
    else
        if dV<0
            Vref=Vrefold-deltaVref;
        else
            Vref=Vrefold+deltaVref;
        end
    end
    else
        Vref=Vrefold;
 end
    if Vref>=Vrefmax/Vref<=Vrefmin
        Vref=Vrefold;
    end
    Vrefold=Vref;
    Vold=V;
    Pold=P;
```